

Project Report
TIP-194

**Covariance Estimation with Scanning
Arrays: FY23 RF Systems Technical
Investment Program**

K. W. Forsythe

21 December 2023

Lincoln Laboratory
MASSACHUSETTS INSTITUTE OF TECHNOLOGY
LEXINGTON, MASSACHUSETTS



DISTRIBUTION STATEMENT A. Approved for public release. Distribution is unlimited.

This material is based upon work supported by the Under Secretary of Defense for Research and Engineering under Air Force Contract No. FA8702-15-D-0001.

This report is the result of studies performed at Lincoln Laboratory, a federally funded research and development center operated by Massachusetts Institute of Technology. This material is based upon work supported by the Under Secretary of Defense for Research and Engineering under Air Force Contract No. FA8702-15-D-0001. Any opinions, findings, conclusions or recommendations expressed in this material are those of the author(s) and do not necessarily reflect the views of the Under Secretary of Defense for Research and Engineering.

© 2023 Massachusetts Institute of Technology

Delivered to the U.S. Government with Unlimited Rights, as defined in DFARS Part 252.227-7013 or 7014 (Feb 2014). Notwithstanding any copyright notice, U.S. Government rights in this work are defined by DFARS 252.227-7013 or DFARS 252.227-7014 as detailed above. Use of this work other than as specifically authorized by the U.S. Government may violate any copyrights that exist in this work.

Massachusetts Institute of Technology
Lincoln Laboratory

Covariance Estimation with Scanning Arrays: FY23 RF
Systems Technical Investment Program

K. W. Forsythe
Group 62

Project Report TIP-194
21 December 2023

DISTRIBUTION STATEMENT A. Approved for public release. Distribution is unlimited.

This material is based upon work supported by the Under Secretary of Defense for Research and Engineering under Air Force Contract No. FA8702-15-D-0001.

Lexington

Massachusetts

This page intentionally left blank.

ABSTRACT

Analog arrays with steerable beams can be capable of angle estimation and sometimes even adaptive beamforming based on power measurements taken at the outputs of multiple beam dwells. In the interesting case of a reflectarray, where beams are formed using a large collection of programmable, passive phase shifters, it is possible to use multiple dwells to estimate signal correlations among the phase shifters. These correlations form an estimated covariance matrix at the phase centers of the shifters. Adaptive beamforming and geolocation can be based on this covariance matrix. Various methods for estimating full-rank and approximately rank-deficient covariance matrices using power measurements from multiple dwells are introduced and evaluated. In some cases, the performance of an estimator can be shown to be optimal in the sense of achieving Cramer-Rao bounds for the estimated covariance parameters.

This page intentionally left blank.

TABLE OF CONTENTS

	Page
Abstract	iii
List of Figures	vii
1. INTRODUCTION	1
2. ESTIMATING COVARIANCE MATRIX ENTRIES	3
3. PING-PONG OPTIMIZATION INCORPORATING SEMI-DEFINITE CONSTRAINTS	7
4. ESTIMATING A RANK-ONE-PLUS-BACKGROUND COVARIANCE	11
4.1 Gauss-Newton Iterations	11
4.2 Performance	12
5. EIGENANALYSIS USING SEQUENTIAL MEASUREMENTS	19
6. DIRECT COVARIANCE ESTIMATION	23
7. SELF-CALIBRATION FOR DISCRETE-VALUED BEAMFORMING WEIGHTS	27
8. DIRECTION-FINDING USING SEQUENTIAL BEAMS	31
9. SUMMARY	39
References	41

This page intentionally left blank.

LIST OF FIGURES

Figure No.		Page
1	<p>One of the key applications for covariance estimation involves the reflectarray shown here. A reflectarray consists of a planar array of quantized phase shifters whose reflected responses are combined at a feed. For our examples using reflectarrays (all but the examples in Section 8), the phase shifters have four distinct, programmable responses. We typically refer to them as 2-bit phase shifters. Beamforming occurs by programming the 2-bit shifters. Since the phase shifters have large dynamic ranges, the shifters can be adjusted to mitigate large interferers that might otherwise challenge the dynamic range of the receiver at the feed. The reflectarray offers both large dynamic range as well as a large number of degrees of freedom to form adaptive and nonadaptive beams.</p>	2
2	<p>Shown are estimates of the first column of the true covariance matrix R, which consists of a single signal with array SNR (ASNR, i.e., SNR including array gain) 40 dB and a noise background modeled by the identity matrix. The first column of R is a standin for the top eigenvector of the covariance. The techniques used for estimating the covariance in general and the first column in particular are treated in Section 2. In this example, $4(n-1)$ measurements are used with the number of shifters equaling $n = 128$. Performance is shown as a function of the number of samples used in each measurement. The separation between the estimate and the first column of the covariance is measured in terms of abstract beamwidths. The beamwidth separation between two vectors v and w is expressed by b, where $\cos(\pi b/2) = \frac{ v^\dagger w }{\ v\ \ w\ }$. Also shown is the Cramer-Rao bound (CRB) associated with estimating the top eigenvector of R. Since beamwidth separation obeys the triangle inequality and since the beamwidth separation between the first column of R and the top eigenvector of R is about $3 \cdot 10^{-4}$, the CRB provides a good indication of how well the first column can be estimated for the values shown in the figure. It is clear that the performance of the estimator is substantially suboptimal and the number of samples/measurement required for good performance is large. Furthermore, performance grows slowly in samples/measurement. As seen later, there are better methods to address these performance drawbacks.</p>	6

LIST OF FIGURES

(Continued)

Figure No.		Page
3	The approximate covariance estimator given by Equ. (6) is evaluated in terms of the number of iterations performed in a fixed scenario consisting of 4000 measurements, with each measurement using 1000 samples. There are 100 2-bit phase shifters in the reflectarray. The covariance's top three eigenvalues are approximately 50, 45, and 40 dB above the noise floor, while the remaining eigenvalues are at the level of the noise floor. For a sense of how close to optimal are the covariance estimates, see Fig. 11 where the same assumptions are made and Cramer-Rao bounds (CRBs) are shown. It is evident from this comparison that the estimator shown here is suboptimal. It does, however, offer a good level of performance and scales well to large numbers of shifters.	9
4	The iteration presented in Equ. (14) is shown here in an example employing a covariance matrix with a single dominant eigenvalue 40 dB above the noise floor, where the remaining eigenvalues are located. The iterations are performed upon collecting 5120 measurements, each measurement using 1000 samples. The reflectarray consists of 892 2-bit phase shifters. Also shown is a CRB based on the Fisher matrix Equ. (12) evaluated using the relations in Equ. (17). To good accuracy, the CRB is achieved by the Gauss-Newton iterations.	14
5	Under the same assumptions as Fig. 4, the CRB is shown as a function of the number of measurements. Recall, each measurement uses 1000 samples. Performance is expressed in terms of the null depth that can be achieved using the estimated principal eigenvector of the covariance. The previous figure shows that these CRBs are achievable. Note that performance is poor below and rapidly improves above a number of measurements equal to a small multiple of the number of shifters (892 here) in the array.	15

LIST OF FIGURES

(Continued)

Figure No.		Page
6	When the interferer exhibits power variations between measurements, the results of Fig. 4 and Fig. 5 can be extended, provided there are auxilliary observations made with an independent phase center. The auxilliary observations track the power variations of the interferer and thus can be used to provide relative values of interference power between measurements at the reflectarray. These estimated (also using 1000 samples) relative values are used in the relations of Equ. (17), requiring only the estimate of a single power parameter p , as before. The example shown uses 256 elements and 5210 measurements of 1000 samples each. The interferer consists of a 40 dB ASNR pulsed signal with 50 percent cycle. The iterations converge similarly to the previous examples, achieving a null depth of 39 dB.	16
7	As a comparison with the pulsed interferer shown in Fig. 6, we show the same example without power variations in the interferer. Far fewer iterations are required for convergence, and the level of performance is better than that of Fig. 6. The achieved null depth is about 46 dB.	17
8	When the interferer pulses in a random manner, performance similar to that of Fig. 6 is achieved. In this case, the null depth is 37 dB.	18
9	The histogram of interference power for the example of Fig. 8 is shown here.	18
10	The sparse eigenanalysis procedure of Section 5 is exercised for a 100-element reflectarray using 4000 measurements of 1000 samples each. The true covariance has three dominant eigenvalues of 50, 45, and 40 dB. All other eigenvalues are at the unity noise floor. Also shown in the figure are CRBs for each of the eigenvalues. The Gauss-Newton iterative procedures introduced in Section 5 hit these bounds after about 200 iterations.	22
11	Since Fig. 10 indicates that the CRBs of sparse eigenanalysis are achievable, the CRBs for various numbers of measurements (number of beams) are shown as an indication of performance variations with the amount of observations. For this example, null depth increases rapidly as the number of measurements per shifter increases beyond 10. The number of measurements per shifter required for good performance tends to scale linearly with the number of significant eigenvalues as long as the eigenvalue sparsity is low as a fraction of the number of shifters.	22

LIST OF FIGURES

(Continued)

Figure No.		Page
12	Direct estimates of the sample covariance as expressed by Equ. (26) are illustrated here for an example similar to those used in Fig. 10 and Fig. 11. The number of measurements per shifter is substantially greater than the number required by the sparse eigenanalysis techniques of Section 5. For example, when measurements/shifter is greater than 10, the results in Fig. 11 show good null depth, while the results here indicate poor null depth unit the ratio is at least 1000.	24
13	Although the covariance estimation procedure of Section 6 is inefficient given sparse eigenvalues, it is robust to variations in the level of interference power that occurs during measurements. The eigenvalue estimates of interferers that pulse with 50 % duty cycles is shown. There is only a few dB loss in null depth compared to Fig. 12.	25
14	Shown is the null depth achieved by an array with 80 3-phase phase shifters. Both curves are based on Fisher matrices for covariance estimation. The deviations from nominal values of the phase shifters is expressed by a calibration residual of -25 dB. Null depth is shown both for the case of perfectly calibrated shifters (known weights) and for the case of unknown and uncalibrated shifters. In the latter case, the unknown calibrations are treated as unknown parameters in a Fisher matrix, with the impact of these unknown nuisance parameters a reduction of null depth. Each power measurement, using a particular set of weight/shifter values, is based on 1000 samples. The measurement weights are randomly chosen. Fluctuations in the curves are due to random changes in true shifter phases (consistent with the calibration error size) and signal array response for each curve point. It is apparent from the size of the fluctuations that these random effects are small.	29
15	The format of Fig. 14 is repeated here with an increase to 256 in the number of phase shifters. The 3 to 4 increase in the number of shifters, over that in Fig. 14, requires about the same increase in the number of measurements to maintain the same level of null depth.	30
16	Shown are the scanning directions of analog beams formed using an 8X8 planar array with half-wavelength element spacing. These steered beams are used to form power estimates of the environment. The estimated powers form the basis of a maximum-likelihood direction-finding algorithm. Shown in green are the beam positions involved in estimating the direction of the source shown in blue.	33

LIST OF FIGURES

(Continued)

Figure No.		Page
17	The beams of Fig. 16 have the shapes and overlaps shown here.	34
18	The maximum-likelihood procedure of Section 8 is employed using the beams and source shown in Fig. 16. Shown is the likelihood statistic. White indicates a starting estimate for the source, red indicates the true source location, black is the peak likelihood, and green shows the settling point the a Gauss-Newton iterative estimator.	35
19	A more challenging example of sequential direction-finding is shown here. The likelihood function is much more complicated, based on measurements from only 6 hexagonally spaced beams (from the same 8X8 planar array) with small overlap. Note the lobe structure showing potential ambiguities in the estimates. As long as the initial estimate (white) is on the correct lobe, the Gauss-Newton estimator converges to a good solution. The colors shown have the same meaning as those in Fig. 18.	36
20	The performance of the iterative estimator on the example shown in Fig. 19 is shown here. The estimator hits the CRB bound. Also shown (as “CRB All”) is the CRB based on sampling the full 8X8 planar array. This shows the loss that could be suffered when using sequential scans instead of multiple, simultaneously sampled phase centers. The beamwidth error measurements are based on the physical definition of beamwidth for the particular array used in the example (8×8 as above) as derived in Section 8 from the abstract definition of beamwidth based on the normalized inner product between array responses.	37

This page intentionally left blank.

1. INTRODUCTION

Covariance estimation using a single scanned beam consumes a large amount of data, particularly for large arrays. Power measurements at the beam outputs are combined in order to estimate components of the covariance matrix. These components include matrix entries as well as eigenvalues and eigenvectors. Measurements are performed by steering the beam with a particular set of array weights, then measuring the power at the beam output given a fixed number of samples. These measurements are repeated many times using different beam weights before any parameter estimates are made. We are interested in techniques that provide efficient (minimal number of samples) estimates and are scalable to large arrays (on the order of one thousand elements). When possible, the performance of all the estimators considered will be compared with appropriate Cramer-Rao bounds.

The array architecture that underlies many of the examples in this report is the reflectarray treated in [MMJ⁺21] and [BCF⁺22]. As shown in Fig. 1, a reflectarray consists of a planar array of passive, quantized (to two bits each in our examples) phase shifters whose reflected signals are combined at a single feed. By programming the phase shifters, various beam patterns can be formed that, for example, suppress interference and provide gain.

This report treats a variety of techniques for covariance estimation and provides a cursory examination of the performance of each approach. Later work will treat relative merits on the basis of concrete measures of performance and complexity in particular applications.

If the covariance is almost rank-deficient in the sense that the covariance matrix is the sum of a known background (the identity matrix here) and a rank-deficient matrix, the number of measurements required for estimation is reduced significantly. In a rough approximation, the number of measurements required for eigenanalysis scales as the rank of the rank-deficient component of the covariance, at least when the almost-rank (rank of the covariance minus the known background contribution) is a small fraction of the total dimension.

We discuss both the estimation of matrix elements as well as the estimation of eigenvalues and eigenvectors. The latter is done mainly for the case of almost rank-deficient covariance matrices. The most thorough and precise results, along with performance bounds, are achieved by using iterative maximum likelihood parameter estimation techniques.

The techniques treated involve direct estimates of matrix entries Section 2, semi-definite programming approaches Section 3, maximum likelihood parameter estimators Section 4, Section 5, and direct estimates of the full covariance Section 6.

The approaches discussed above rely on some form of calibration to model the responses of the phase shifters that provide the weights for each array element. If these responses are not known, they can be fit exactly (assuming angle-independent phase states) with simple polynomial models of the finite number of phase states at each phase shifter. The nuisance parameters associated with this self-calibration approach must be estimated in addition to the usual covariance parameters. The effect of this kind of self-calibration on Cramer-Rao performance bounds for covariance estimation is treated in Section 7 in the rank-one case.

Finally, in Section 8, we provide a cursory treatment of geolocation using scanned beams for planar arrays. The approach taken there is exclusively maximum likelihood parameter estimation.

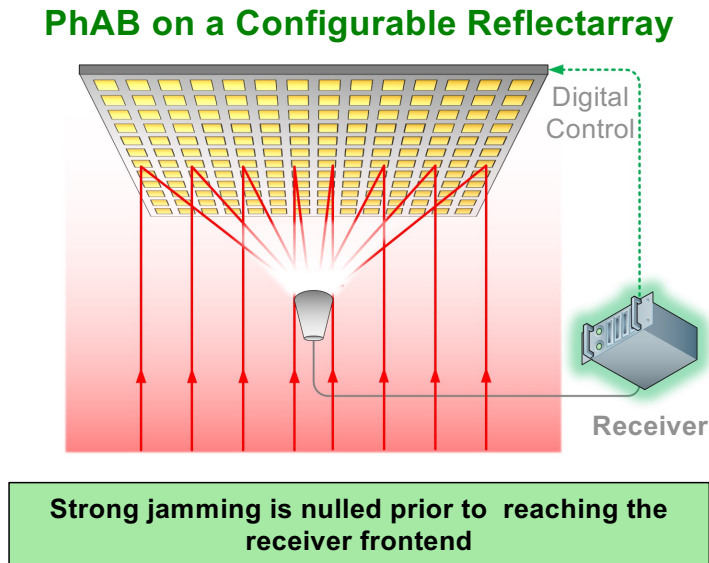


Figure 1. One of the key applications for covariance estimation involves the reflectarray shown here. A reflectarray consists of a planar array of quantized phase shifters whose reflected responses are combined at a feed. For our examples using reflectarrays (all but the examples in Section 8), the phase shifters have four distinct, programmable responses. We typically refer to them as 2-bit phase shifters. Beamforming occurs by programming the 2-bit shifters. Since the phase shifters have large dynamic ranges, the shifters can be adjusted to mitigate large interferers that might otherwise challenge the dynamic range of the receiver at the feed. The reflectarray offers both large dynamic range as well as a large number of degrees of freedom to form adaptive and nonadaptive beams.

2. ESTIMATING COVARIANCE MATRIX ENTRIES

It is possible to find simple expressions that provide estimates of the entries of a covariance matrix based solely on power measurements. We begin by treating a two-element ($n = 2$) case and then extend the results. The focus quickly becomes estimating the first column of the covariance matrix. When there is a single strong signal in the covariance, the array response of the signal is closely approximated by the first column of the matrix. The accuracy of the matrix-element estimators treated is examined and compared with a Cramer-Rao bound, which is computed in a later section. One should keep in mind the example array of Fig. 1.

The results in this section consider the estimation of entries in the covariance matrix that could be formed between phase shifters if these shifters had each acted as individual sensors and been sampled independently. Such estimated covariances can be used as the basis of beamforming. The covariance matrix entries are estimated by combining power measurements taken using various combinations of shifter settings. Below, for convenience, the 2-bit phase shifters are assumed to take the four values $\pm i, \pm 1$.

The following expressions handle the case of two phase shifters, $n = 2$. Let $\mathbf{z} = (z_1, z_2)^T$ denote a complex 2-vector. We have the relations.

$$\frac{\mathbb{E}[|z_1 + z_2|^2] - \mathbb{E}[|z_1 - z_2|^2]}{4} = \Re \mathbb{E}[z_1 \bar{z}_2]$$

and

$$\frac{\mathbb{E}[|z_1 - iz_2|^2] - \mathbb{E}[|z_1 + iz_2|^2]}{4} = \Im \mathbb{E}[z_1 \bar{z}_2]$$

Define

$$p_{\pm} \stackrel{\text{def}}{=} \mathbb{E}[|z_1 \pm z_2|^2]$$

and

$$q_{\pm} \stackrel{\text{def}}{=} \mathbb{E}[|z_1 \pm iz_2|^2]$$

Then

$$\mathbb{E}[z_1 \bar{z}_2] = \frac{(p_+ - p_-)}{4} + i \frac{(q_- - q_+)}{4}$$

with the relation

$$(p_+ - p_-) - (q_- - q_+) = 0$$

All power estimates have the form $\mathbb{E}[|\mathbf{w}^\dagger \mathbf{z}|^2] = \mathbf{w}^\dagger \mathbf{R} \mathbf{w}$ with $w_k \in \{1, -1, i, -i\}$. We define $\mathcal{C} \stackrel{\text{def}}{=} \{\mathbf{w} | w_k \in \{1, -1, i, -i\}\}$. The particular discrete values taken by the w_k are arbitrarily chosen in the following as a representative, practical set, but the form of the analysis extends to more general choices.

If $\text{tr} \mathbf{A} = 0$ with real, diagonal \mathbf{A} , then $\mathbf{w}^\dagger \mathbf{A} \mathbf{w} = \sum_k A_{kk} w_k^2 = 0$ when $\mathbf{w} \in \mathcal{C}$. In consequence, all power estimates with weights from \mathcal{C} are insensitive to traceless diagonal matrices. If the cost function for adapting a weight only involves the covariance \mathbf{R} through power expressions of the form $\mathbf{w}^\dagger \mathbf{R} \mathbf{w}$ with $\mathbf{w} \in \mathcal{C}$, then the inability to estimate the traceless diagonal components of \mathbf{R} does not effect adaptation.

One way to estimate \mathbf{R} evaluates $\text{tr}(\mathbf{R}\mathbf{w}\mathbf{w}^\dagger)$ for n^2 weights \mathbf{w} since the linear dimension of hermitian matrices is n^2 . But what we have just mentioned, the span of matrices of the form $\mathbf{w}\mathbf{w}^\dagger$ with $\mathbf{w} \in \mathcal{C}$ is at most $n^2 - n + 1$ since the $n - 1$ dimensional space of traceless diagonal matrices cannot be estimated. Thus, assuming for the moments that $\text{dimspan}\{\mathbf{w}\mathbf{w}^\dagger | \mathbf{w} \in \mathcal{C}\} = n^2 - n + 1$, this is the minimal number of measurements required.

Next, we illustrate how to systematically estimated the entries $\{R_{12}, R_{13}, \dots, R_{1n}\}$ of \mathbf{R} . This procedure can be applied to other rows, showing that all off-diagonal elements of R can be estimated. Define

$$Q(\mathbf{w}) \stackrel{\text{def}}{=} \begin{pmatrix} 1 \\ \mathbf{w} \end{pmatrix}^\dagger \mathbf{R} \begin{pmatrix} 1 \\ w \end{pmatrix}.$$

We have

$$\frac{Q(\mathbf{w}) - Q(-\mathbf{w})}{2} = \text{tr}(\mathbf{E}_w \mathbf{R})$$

and

$$\frac{Q(-i\mathbf{w}) - Q(i\mathbf{w})}{2} = \text{tr}(\mathbf{F}_w \mathbf{R})$$

with hermitian matrices $\mathbf{E}_w, \mathbf{F}_w$ defined as follows:

$$\mathbf{E}_w \stackrel{\text{def}}{=} \frac{1}{2} \left[\begin{pmatrix} 1 \\ 0 \end{pmatrix} \begin{pmatrix} 0 \\ \mathbf{w} \end{pmatrix}^\dagger + \begin{pmatrix} 0 \\ \mathbf{w} \end{pmatrix} \begin{pmatrix} 1 \\ 0 \end{pmatrix}^\dagger \right]$$

and

$$\mathbf{F}_w \stackrel{\text{def}}{=} \frac{i}{2} \left[\begin{pmatrix} 1 \\ 0 \end{pmatrix} \begin{pmatrix} 0 \\ \mathbf{w} \end{pmatrix}^\dagger - \begin{pmatrix} 0 \\ \mathbf{w} \end{pmatrix} \begin{pmatrix} 1 \\ 0 \end{pmatrix}^\dagger \right].$$

In consequence,

$$\begin{pmatrix} 1 \\ 0 \end{pmatrix}^\dagger \mathbf{R} \begin{pmatrix} 0 \\ \mathbf{w} \end{pmatrix} = \text{tr}[(\mathbf{E}_w + i\mathbf{F}_w)\mathbf{R}].$$

Denote the standard basis vectors \mathbf{e}_k (single unity entry k and all others zero) for the $n - 1$ dimensional Euclidian space. We can write $\mathbf{e}_k = \sum_l b_{kl} \mathbf{w}_l$ for some $n - 1$ $\mathbf{w}_l \in \mathcal{C}$. Thus, we have

$$R_{1k} = \sum_l b_{kl} \text{tr}[(\mathbf{E}_{w_l} + i\mathbf{F}_{w_l})\mathbf{R}].$$

Assuming we can estimate $\text{tr} \mathbf{R}$ with n measurements, the total number of power measurements required to estimate \mathbf{R} (up to degeneracy) is expressed by $4 \cdot (n - 1) \cdot n + n = 4n^2 - 3n$. If we take advantage of the fact that we get redundant estimates from succeeding row estimates, we need instead $4 \cdot [(n - 1) + (n - 2) + \dots + 1] + n = 2n^2 - n$ power measurements.

To estimate the trace of \mathbf{R} , assume that $n = 2^m$ and let \mathbf{H} denote the $n \times n$ Hadamard matrix with ± 1 entries. Form

$$\text{tr}(\mathbf{H}\mathbf{R}\mathbf{H}^\dagger) = n \text{tr}(\mathbf{R})$$

which expresses the sum of the n power measurements associated with the weights provided by the rows of \mathbf{H} .

A power measurement of the form $\mathbf{w}^\dagger \mathbf{R} \mathbf{w}$, is estimated by the random variable $L^{-1} \sum_l |\mathbf{w}^\dagger \mathbf{z}_l|^2$ with unbiased mean $\mathbf{w}^\dagger \mathbf{R} \mathbf{w}$ and covariance $(\mathbf{w}^\dagger \mathbf{R} \mathbf{w})^2/L$, under the assumption that the \mathbf{z}_l are i.i.d. complex Gaussian random vectors with covariance \mathbf{R} . This means that the estimate of $\text{tr} \mathbf{R}$ is unbiased with covariance

$$\frac{1}{nL} \text{tr}((\mathbf{H} \mathbf{R} \mathbf{H}^\dagger) \circ (\mathbf{H} \mathbf{R} \mathbf{H}^\dagger))$$

where $\mathbf{A} \circ \mathbf{B}$ expresses the adamard (entry-by-entry) product of two matrices.

To investigate the effects of measurement errors on the off-diagonal entries of an estimated \mathbf{R} , let $\hat{Q}(\mathbf{w}) \stackrel{\text{def}}{=} L^{-1} \sum_l |(1, \mathbf{w}^\dagger) \mathbf{z}_l|^2$. This estimator is unbiased with covariance $Q(\mathbf{w})^2/L$. If we let $\mathbf{r} \stackrel{\text{def}}{=} (\hat{\mathbf{R}}_{12}, \dots, \hat{\mathbf{R}}_{1n})^T$, then the estimates of the first row of \mathbf{R} have the form

$$\mathbf{r} = \mathbf{B}(\mathbf{a} + i\mathbf{b})$$

where

$$\mathbb{E}[a_l] = \frac{Q(\mathbf{w}_l) - Q(-\mathbf{w}_l)}{2}$$

and

$$\text{cov}(a_l) = \frac{Q^2(\mathbf{w}_l) + Q^2(-\mathbf{w}_l)}{4L}.$$

Similarly,

$$\mathbb{E}[b_l] = \frac{Q(-i\mathbf{w}_l) - Q(i\mathbf{w}_l)}{2}$$

and

$$\text{cov}(b_l) = \frac{Q^2(-i\mathbf{w}_l) + Q^2(i\mathbf{w}_l)}{4L}.$$

Since the cross-covariance of \mathbf{a} and \mathbf{b} vanishes, we can write

$$\text{cov}_T(\mathbf{r}) \stackrel{\text{def}}{=} \mathbb{E}[\mathbf{r} \mathbf{r}^T] - \mathbb{E}[\mathbf{r}] \mathbb{E}[\mathbf{r}]^T = B (\text{cov}[\mathbf{a}] - \text{cov}[\mathbf{b}]) B^T$$

and

$$\text{cov}_H(\mathbf{r}) \stackrel{\text{def}}{=} \mathbb{E}[\mathbf{r} \mathbf{r}^\dagger] - \mathbb{E}[\mathbf{r}] \mathbb{E}[\mathbf{r}]^\dagger = B (\text{cov}[\mathbf{a}] + \text{cov}[\mathbf{b}]) B^\dagger.$$

Note that $\text{cov}(\mathbf{a})$, etc. are real diagonal matrices.

More generally, if we let $\mathbf{r} = \mathbf{r}_I + i\mathbf{r}_Q$ decompose \mathbf{r} into real and imaginary components, we have

$$\Re(\text{cov}_H(\mathbf{r}) \pm \text{cov}_T(\mathbf{r})) = \begin{cases} \text{cov}(\mathbf{r}_I) \\ \text{cov}(\mathbf{r}_Q) \end{cases}$$

and

$$\Im(\text{cov}_T(\mathbf{r}) - \text{cov}_H(\mathbf{r})) = \text{cov}(\mathbf{r}_I, \mathbf{r}_Q) = \mathbb{E}[\mathbf{r}_I \mathbf{r}_Q^T] - \mathbb{E}[\mathbf{r}_I] \mathbb{E}[\mathbf{r}_Q]^T.$$

The equations above together give us the ability to evaluate the covariance of the complex estimated vector \mathbf{r} .

We can apply the methods above to estimating the first column of the covariance matrix associated with an almost rank one matrix. In other words, the true covariance is the sum of a rank-one matrix and the identity matrix. When the rank-one summand is large, the estimator behaves as shown in the example Fig. 2. This type of estimator falls short of what may be achieved as shown by the comparison with a Cramer-Rao bound.

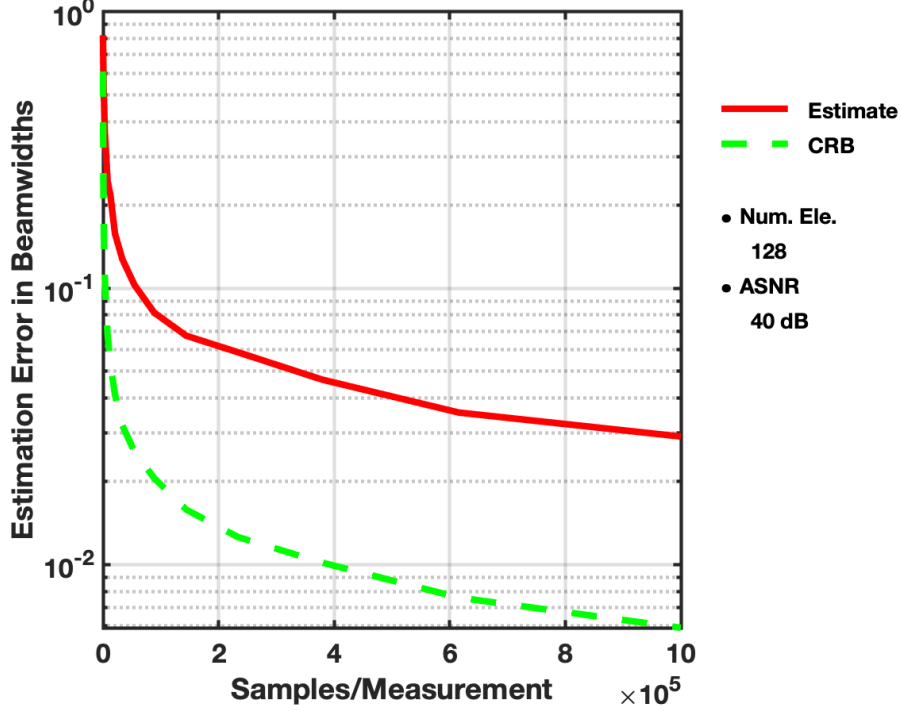


Figure 2. Shown are estimates of the first column of the true covariance matrix R , which consists of a single signal with array SNR (ASNR, i.e., SNR including array gain) 40 dB and a noise background modeled by the identity matrix. The first column of R is a standin for the top eigenvector of the covariance. The techniques used for estimating the covariance in general and the first column in particular are treated in Section 2. In this example, $4(n - 1)$ measurements are used with the number of shifters equaling $n = 128$. Performance is shown as a function of the number of samples used in each measurement. The separation between the estimate and the first column of the covariance is measured in terms of abstract beamwidths. The beamwidth separation between two vectors v and w is expressed by b , where $\cos(\pi b/2) = \frac{|v^\dagger w|}{\|v\| \|w\|}$. Also shown is the Cramer-Rao bound (CRB) associated with estimating the top eigenvector of R . Since beamwidth separation obeys the triangle inequality and since the beamwidth separation between the first column of R and the top eigenvector of R is about $3 \cdot 10^{-4}$, the CRB provides a good indication of how well the first column can be estimated for the values shown in the figure. It is clear that the performance of the estimator is substantially suboptimal and the number of samples/measurement required for good performance is large. Furthermore, performance grows slowly in samples/measurement. As seen later, there are better methods to address these performance drawbacks.

3. PING-PONG OPTIMIZATION INCORPORATING SEMI-DEFINITE CONSTRAINTS

Semi-definite programming techniques are an obvious candidate for estimating covariance matrices. These approaches find positive semi-definite matrices that fit the measurements. We use a least-squares fit to the measurements combined with a decoupled semi-definite constraint to form a simple iterative algorithm.

In the following, power measurements \hat{p}_k are taken with weights \mathbf{w}_k . The measurements have the form $\mathbf{w}_k^\dagger \mathbf{Y} \mathbf{w}_k$ for an unconstrained hermitian \mathbf{Y} which is fit to a positive semi-definite (p.s.d.) approximation \mathbf{X} . The two estimates are coupled by a weighting μ .

Consider the estimate of p.s.d. \mathbf{X} in the complex case by solving iteratively ($\|\cdot\|_F$ denotes Frobenius norm)

$$\min_{\mathbf{X} \geq 0, \mathbf{Y} = \mathbf{Y}^\dagger} \|\mathbf{X} - \mathbf{Y}\|_F^2 + \mu \sum_k (\mathbf{w}_k^\dagger \mathbf{Y} \mathbf{w}_k - \hat{p}_k)^2. \quad (1)$$

The LS problem in \mathbf{Y} can be solved by completing the square, while the LS problem for \mathbf{X} , fixing \mathbf{Y} , is simply $\mathbf{X} = \mathbf{Y}^+$, the projection onto the convex cone of p.s.d. complex hermitian matrices. This leads to the iterative procedure

$$\begin{aligned} \text{Vec}(\hat{\mathbf{Y}}) &= \left(I_n + \mu \sum_k \text{Vec}(\mathbf{w}_k \mathbf{w}_k^\dagger) \text{Vec}(\mathbf{w}_k \mathbf{w}_k^\dagger)^\dagger \right)^{-1} \left(\text{Vec}(\mathbf{X}) + \mu \sum_k \hat{p}_k \text{Vec}(\mathbf{w}_k \mathbf{w}_k^\dagger) \right) \\ \hat{\mathbf{X}} &= \hat{\mathbf{Y}}^+. \end{aligned} \quad (2)$$

To see this, write $\mathbf{X}_V \stackrel{\text{def}}{=} \text{Vec}(\mathbf{X})$ and $\mathbf{Y}_V \stackrel{\text{def}}{=} \text{Vec}(\mathbf{Y})$ where $\text{Vec}(\cdot)$ unwraps its matrix argument by rows (beware, the usual definition of Vec unwraps by columns). Also use the definition

$$\mathbf{C}_V = \mathbf{I} + \mu \sum_k \text{Vec}(\mathbf{w}_k \mathbf{w}_k^\dagger) \text{Vec}(\mathbf{w}_k \mathbf{w}_k^\dagger)^\dagger \quad (3)$$

and the identity

$$\text{Vec}(\mathbf{X})^\dagger \text{Vec}(\mathbf{Y}) = \text{tr}(\mathbf{X}^\dagger \mathbf{Y}) = \text{tr}(\mathbf{X} \mathbf{Y}) \in \mathbb{R}. \quad (4)$$

This leads us to rewrite Equ. (1) as

$$\left(\mathbf{Y}_V - \mathbf{C}_V^{-1} \left(\mu \text{Vec} \left(\sum_k \hat{p}_k \mathbf{w}_k \mathbf{w}_k^\dagger \right) + \mathbf{X}_V \right) \right)^\dagger \mathbf{C}_V \left(\mathbf{Y}_V - \mathbf{C}_V^{-1} \left(\mu \text{Vec} \left(\sum_k \hat{p}_k \mathbf{w}_k \mathbf{w}_k^\dagger \right) + \mathbf{X}_V \right) \right) + \text{O.T.}, \quad (5)$$

where O.T. stand for other terms that don't involve \mathbf{Y}_V . The first line of Equ. (2) follows.

For $0 < \mu \ll 1$, the update steps of Equ. (2) can be approximated by

$$\begin{aligned} \hat{\mathbf{Y}} &= \mathbf{X} - \mu \sum_k (\mathbf{w}_k^\dagger \mathbf{X} \mathbf{w}_k - \hat{p}_k) \mathbf{w}_k \mathbf{w}_k^\dagger \\ \hat{\mathbf{X}} &= \mathbf{Y}^+. \end{aligned} \quad (6)$$

The approximation is chosen to avoid the matrix inversion implicit in the true update step. This short-cut, motivated by using an approximate inverse, is chosen to obtain good scaling behavior to larger matrix dimensions.

An example of the performance of the iterative optimization Equ. (6) of the semi-definite statistic of Equ. (1) is shown in Fig. 3. This technique scales well to a large number of elements and has good performance as measured by the null depth achieved on each of the three signals used in the example. The signals have array SNRs (ASNR) of 50, 45, and 40 dB. Shown is the null depth achieved on each signal. Recall that the ASNR of a signal is the SNR at the output of a beam pointed at the signal in the absence of interference but in the presence of the noise background.

The projection onto the cone of complex, positive semi-definite covariances indicated in Equ. (6) can be replaced by projection onto the space spanned by the top eigenvectors of \mathbf{Y} . This reduces the computational burden for large matrices while still addressing the almost rank-deficient matrices of interest here. The results shown in Fig. 3 project onto a three-dimensional eigenspace in the step $\hat{\mathbf{X}} = \mathbf{Y}^+$.

Since the array responses of the signals in the example of Fig. 3 are nearly orthogonal (due in part to the large number of elements), these array responses are approximately the eigenvectors of the rank-deficient summand of the covariance. This allows us to use the techniques of Section 5 to compare the eigenvector estimates obtained from Equ. (1) with those obtained from a Cramer-Rao bound. Given 40 beams/shifter, the CRBs shown in Fig. 11 indicate null depths of about -43, -36, and -27 dB, compared to the null depths of -36, -30, and -20 dB obtained from Fig. 3, which are about 7 dB worse than optimal.

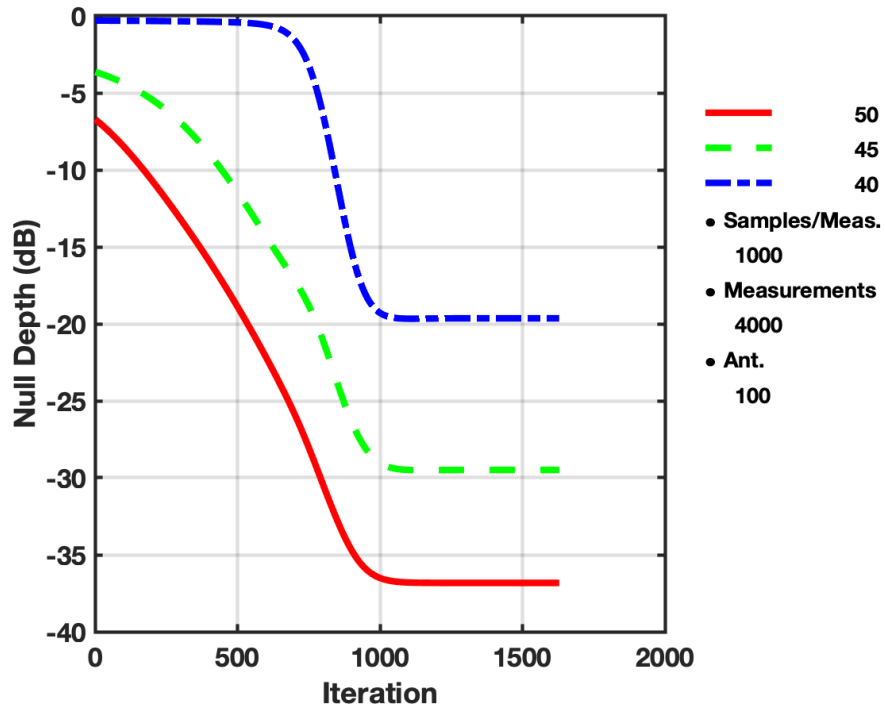


Figure 3. The approximate covariance estimator given by Equ. (6) is evaluated in terms of the number of iterations performed in a fixed scenario consisting of 4000 measurements, with each measurement using 1000 samples. There are 100 2-bit phase shifters in the reflectarray. The covariance's top three eigenvalues are approximately 50, 45, and 40 dB above the noise floor, while the remaining eigenvalues are at the level of the noise floor. For a sense of how close to optimal are the covariance estimates, see Fig. 11 where the same assumptions are made and Cramer-Rao bounds (CRBs) are shown. It is evident from this comparison that the estimator shown here is suboptimal. It does, however, offer a good level of performance and scales well to large numbers of shifters.

This page intentionally left blank.

4. ESTIMATING A RANK-ONE-PLUS-BACKGROUND COVARIANCE

After a brief review of a Gaussian likelihood for narrowband array data and the associated Fisher matrices, we specialize to a particular parameterized model of the covariance matrix that treats an almost rank-one covariance with unknown top eigenvalue and eigenvector, which are both to be estimated. Estimation follows an iterative procedure that employs a Gauss-Newton update step based on the calculation of the Fisher matrix. Results are complete but the arguments are only sketched. It may be helpful, in the course of reading this section, to glance at the beginning of Section 8 where a more concrete direction-finding problem is treated in an analogous manner.

4.1 GAUSS-NEWTON ITERATIONS

Assuming parameters live in the covariance, we have the narrowband Gaussian signal PDF for the data \mathbf{Z} conditioned on the covariance \mathbf{R}

$$p(\mathbf{Z}|\mathbf{R}) = \pi^{-nl} |\mathbf{R}|^{-l} e^{-l \text{tr} \mathbf{R}^{-1} \mathbf{Z} \mathbf{Z}^\dagger / l}. \quad (7)$$

Its derivatives are expressed by ($\dot{\mathbf{R}}$ denotes derivative by an unspecified parameter and $\hat{\mathbf{R}} \stackrel{\text{def}}{=} \mathbf{Z} \mathbf{Z}^\dagger / l$)

$$\partial_R \log p(\mathbf{Z}|\mathbf{R}) = l \left(-\partial_R \log |\mathbf{R}| - \partial_R \text{tr} \mathbf{R}^{-1} \hat{\mathbf{R}} \right) = l \left(-\text{tr} \mathbf{R}^{-1} \dot{\mathbf{R}} + \text{tr} \mathbf{R}^{-1} \dot{\mathbf{R}} \mathbf{R}^{-1} \hat{\mathbf{R}} \right). \quad (8)$$

This leads to a gradient of the form

$$\mathbf{g} \stackrel{\text{def}}{=} \nabla \log p(\mathbf{Z}|\mathbf{R}) \leftrightarrow l \left(\mathbf{R}^{-1} \hat{\mathbf{R}} \mathbf{R}^{-1} - \mathbf{R}^{-1} \right) \quad (9)$$

based on the inner product $\langle A, B \rangle \stackrel{\text{def}}{=} \text{tr}(AB)$. In explicit terms, the component of gradient ($\mathbf{R}_j \stackrel{\text{def}}{=} \partial_j \mathbf{R}$) becomes

$$g_j = \text{tr}((\nabla \log p(\mathbf{Z}|\mathbf{R})) \mathbf{R}_j) = \text{tr}(l(\mathbf{R}^{-1} \hat{\mathbf{R}} \mathbf{R}^{-1} - \mathbf{R}^{-1}) \mathbf{R}_j). \quad (10)$$

Abusing notation by letting $\dot{\mathbf{R}}$ represent different partial derivatives, we have

$$\partial_R^2 \log p(\mathbf{Z}|\mathbf{R}) = -l \text{tr}(\dot{\mathbf{R}} \mathbf{R}^{-1} \dot{\mathbf{R}} \mathbf{R}^{-1}) - 2 \text{tr}(\mathbf{R}^{-1} \dot{\mathbf{R}} \mathbf{R}^{-1} \dot{\mathbf{R}} \mathbf{R}^{-1} \mathbf{Z} \mathbf{Z}^\dagger). \quad (11)$$

Taking expectations (and using $\mathbb{E}[\mathbf{Z} \mathbf{Z}^\dagger] = l \mathbf{R}$), we arrive at $l \text{tr}(\mathbf{R}^{-1} \dot{\mathbf{R}} \mathbf{R}^{-1} \dot{\mathbf{R}})$. Thus, the Fisher becomes

$$F_{ij} = -\mathbb{E}[\partial_i \partial_j \log p(\mathbf{Z}|\mathbf{R})] = l \text{tr}(\mathbf{R}^{-1} \mathbf{R}_i \mathbf{R}^{-1} \mathbf{R}_j). \quad (12)$$

To perform Gauss-Newton iteration, we first consider the approximation

$$\begin{aligned} \log p(\mathbf{Z}|\mathbf{R} + \sum \mathbf{R}_i \delta_i) &\approx \log p(\mathbf{Z}|\mathbf{R}) + l \text{tr}[(\mathbf{R}^{-1} \hat{\mathbf{R}} \mathbf{R}^{-1} - \mathbf{R}^{-1}) \sum \mathbf{R}_i \delta_i] - \frac{l}{2} \text{tr}(\mathbf{R}^{-1} \mathbf{R}_i \mathbf{R}^{-1} \mathbf{R}_j) \delta_i \delta_j \\ &= \text{const.} + \mathbf{g} \cdot \delta - \frac{1}{2} \delta^T \mathbf{F} \delta = \text{const.} - (\delta - \mathbf{F}^{-1} \mathbf{g})^T \mathbf{F} (\delta - \mathbf{F}^{-1} \mathbf{g}) / 2. \end{aligned} \quad (13)$$

The Gauss-Newton update step becomes

$$\delta \leftarrow \delta + \mu \mathbf{F}^{-1} \mathbf{g}. \quad (14)$$

Next, we consider coordinates for the almost rank-one covariance matrix \mathbf{R} . Assume $\mathbf{R} = I_n + p\mathbf{v}\mathbf{v}^\dagger$ with $\|\mathbf{v}\| = 1$. For now, assume $\mathbf{v} = \mathbf{e}_1$. The vector \mathbf{e}_k denotes the all zeros vector except for unity in the k^{th} component. The parameters are $p = a^2$ and b_j, \tilde{b}_j parameterizing unitaries that rotate $\mathbf{e}_1, \mathbf{e}_2$ (and leave the orthocomplement of \mathbf{e}_1 and \mathbf{e}_2 unchanged) as follows:

$$\begin{aligned} \mathbf{U}_j &\text{ takes } \mathbf{e}_1 \text{ to } \cos(\pi b_j/2)\mathbf{e}_1 + \sin(\pi b_j/2)\mathbf{e}_j \\ \tilde{\mathbf{U}}_j &\text{ takes } \mathbf{e}_1 \text{ to } \cos(\pi \tilde{b}_j/2)\mathbf{e}_1 + i \sin(\pi \tilde{b}_j/2)\mathbf{e}_j \end{aligned} \quad (15)$$

$$\mathbf{v}(\mathbf{b}, \tilde{\mathbf{b}}) = \left(\prod_j \mathbf{U}_j \tilde{\mathbf{U}}_j \right) \mathbf{e}_1. \quad (16)$$

We need to evaluate derivatives of Equ. (16) at $\mathbf{b} = 0 = \tilde{\mathbf{b}}$ where the \mathbf{U}_j and $\tilde{\mathbf{U}}_j$ are identity operators, so the order of the factors in the products over \mathbf{U}_j and $\tilde{\mathbf{U}}_j$ doesn't matter. The derivatives by angle and amplitude parameters as well as inner products, evaluated at $\mathbf{b} = 0 = \tilde{\mathbf{b}}$, become

$$\begin{aligned} \mathbf{R}_j &= \partial_{b_j} \mathbf{R} = \frac{\pi p}{2} (\mathbf{e}_1 \mathbf{e}_j^\dagger + \mathbf{e}_j \mathbf{e}_1^\dagger) \\ \tilde{\mathbf{R}}_j &= \partial_{\tilde{b}_j} \mathbf{R} = \frac{i\pi p}{2} (\mathbf{e}_1 \mathbf{e}_j^\dagger - \mathbf{e}_j \mathbf{e}_1^\dagger) \\ \mathbf{R}_a &= \partial_a \mathbf{R} = 2a \mathbf{e}_1 \mathbf{e}_1^\dagger \\ 0_{j \neq k} = \text{tr}(\mathbf{R}_j \mathbf{R}_k) &= \text{tr}(\tilde{\mathbf{R}}_j \tilde{\mathbf{R}}_k) = \text{tr}(\tilde{\mathbf{R}}_j \mathbf{R}_k) \\ \text{tr} \mathbf{R}_j^2 &= \frac{p^2 \pi^2}{2} = \text{tr} \tilde{\mathbf{R}}_j^2 \end{aligned} \quad (17)$$

Gauss-Newton updates can be based on the above expressions, specialized to the covariances of interest. For covariance estimation based on power measurements, these covariances have the form $\mathbf{w}^\dagger \mathbf{R} \mathbf{w}$ for varying weights \mathbf{w} . The model is still based on the full covariance \mathbf{R} , even though it is never directly observed. See Section 8 for a more concrete description in a related application.

The updates are based on $\mathbf{v} = \mathbf{e}_1$, but any current estimate of a different \mathbf{v} can be rotated using a unitary to \mathbf{e}_1 , the update applied, and then the result rotated back. The unitaries preserve the geometry, which is homogeneous and locally orthonormal up to a scale factor.

4.2 PERFORMANCE

In Fig. 4 we show convergence of the Gauss-Newton iterator to the eigenvector of an almost rank-one covariance with a principal eigenvalue of 40 dB. The example is based on 5120 measurements of 1000 samples each for an array consisting of 892 2-bit phase shifters. Accuracy of the estimates are measured in terms of the beamwidth separation between estimate and truth. The beamwidth separation b between two complex n -vectors is associated with the absolute value of the normalized inner product between the vectors as expressed by $\cos(\pi b/2)$. The initial estimate of the eigenvector that seeds the iteration is within about 1/2 beamwidth of the true eigenvector. In practice, scanning the beam can provide crude (within a beamwidth) estimates to see iterative refinements. Also shown in the figure is a Cramer-Rao bound (CRB) on the performance of an unbiased estimator, as derived above. The Gauss-Newton iterator achieves this CRB.

In Fig. 5, the convergence performance of the Gauss-Newton estimator is characterized by a CRB. Performance is shown as a function of the number of measurements, with a fixed number of samples used for the power estimates in each measurement. Performance is poor until the number of measurements exceeds a small multiple of the number of phase shifters, after which it improves rapidly.

In the performance charts, the signals are assumed to be stationary. We can treat a signal with varying interference power by adding a new (notionally omnidirectional) sensor to the array that can make power measurements coordinated with the power measurements taken with each fixed set of phase shifter weights. In this manner, the measurement-to-measurement variations on signal power can be tracked. The rank-one covariance model still has a single unknown amplitude parameter for the signal, but scales the signal power measurement-to-measurement according to the power measurements on the auxiliary omni.

With these modifications to the estimator, a pulsed interferer can be estimated in the case of an almost rank-one covariance. In Fig. 6, we show an example with a 50% duty factor signal impinging on a 256 element array of 2-bit phase shifters. Again, there are 5210 measurements of 1000 samples each. The results show convergence after close to 1000 iterations. The null depth is expressed by $\sin^2(\pi b/2)$, where b is the separation in beamwidths between the estimate and truth. In this example, the null depth is 39 dB. For comparison, Fig. 7 shows a Gauss-Newton iteration when the interferer is stationary. Convergence is faster by more than an order of magnitude and the level of performance is better, showing 46 dB null depth as opposed to 39 dB.

In Fig. 8 we show performance for an intermittent interferer that has a power histogram as shown in Fig. 9. Performance is similar to that shown in Fig. 6, with a null depth of about 37 dB.

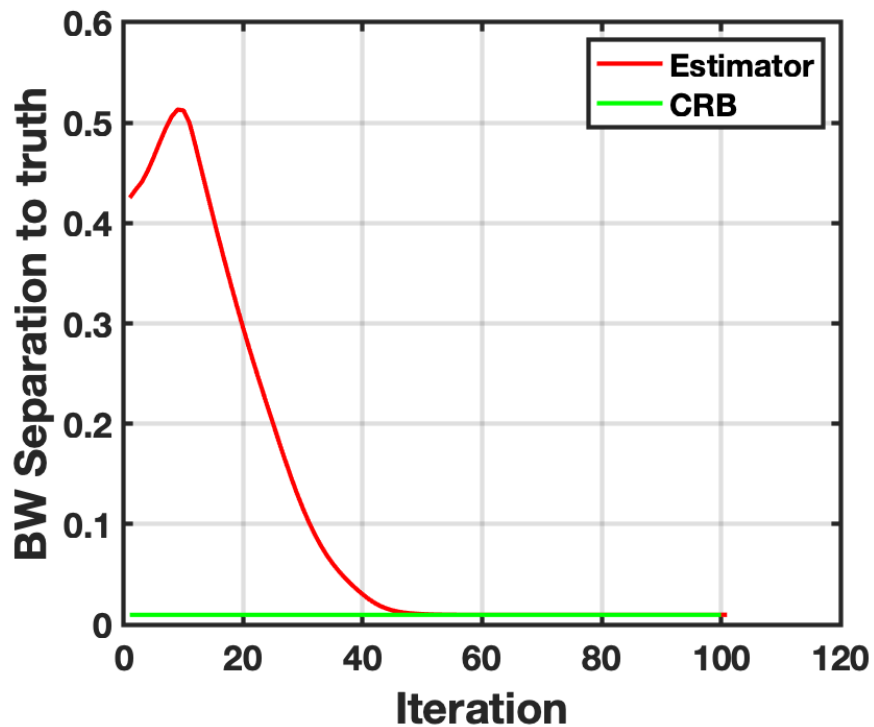


Figure 4. The iteration presented in Equ. (14) is shown here in an example employing a covariance matrix with a single dominant eigenvalue 40 dB above the noise floor, where the remaining eigenvalues are located. The iterations are performed upon collecting 5120 measurements, each measurement using 1000 samples. The reflectarray consists of 892 2-bit phase shifters. Also shown is a CRB based on the Fisher matrix Equ. (12) evaluated using the relations in Equ. (17). To good accuracy, the CRB is achieved by the Gauss-Newton iterations.

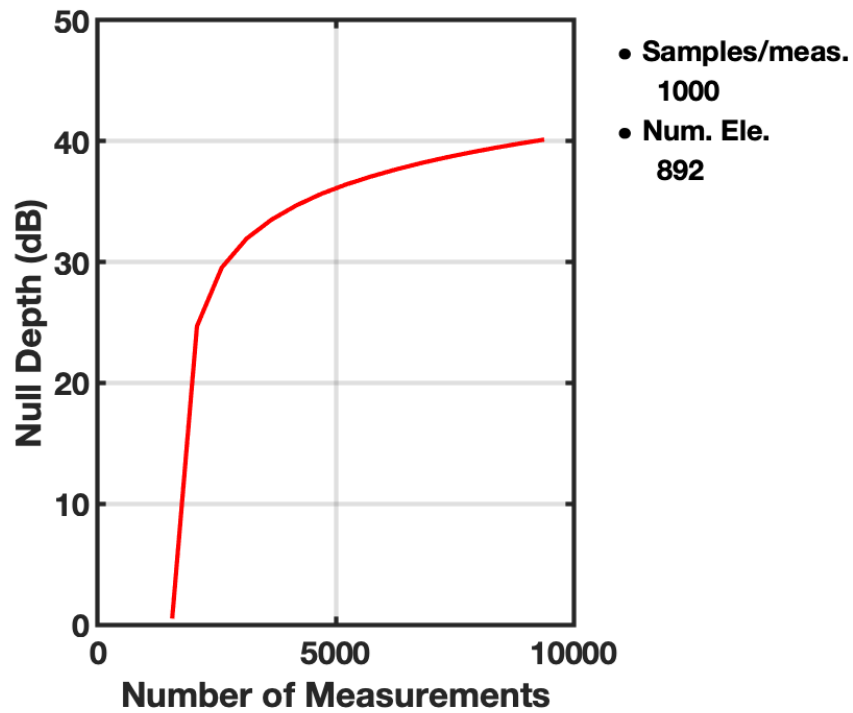


Figure 5. Under the same assumptions as Fig. 4, the CRB is shown as a function of the number of measurements. Recall, each measurement uses 1000 samples. Performance is expressed in terms of the null depth that can be achieved using the estimated principal eigenvector of the covariance. The previous figure shows that these CRBs are achievable. Note that performance is poor below and rapidly improves above a number of measurements equal to a small multiple of the number of shifters (892 here) in the array.

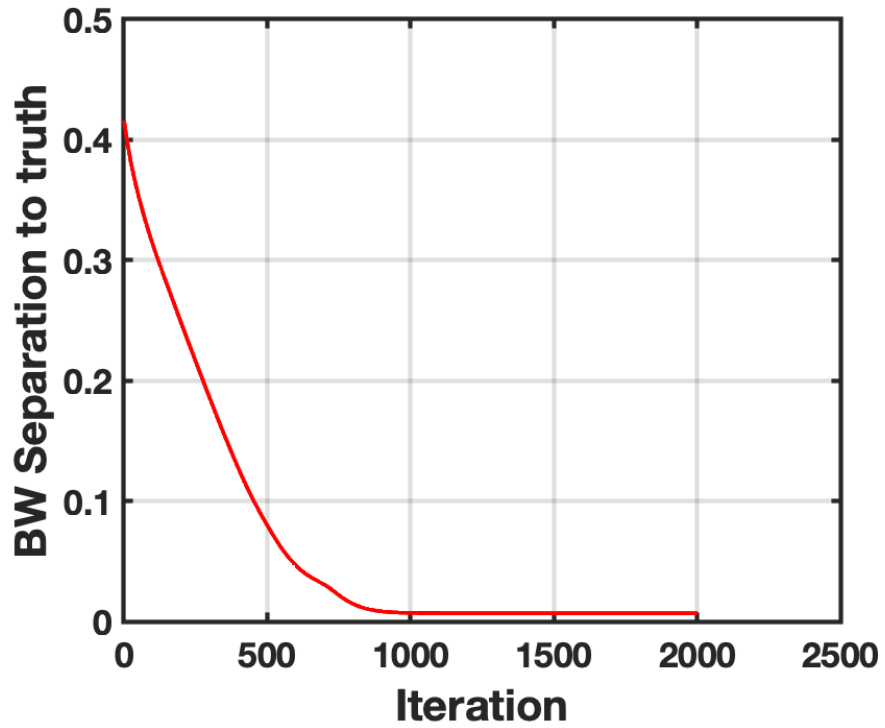


Figure 6. When the interferer exhibits power variations between measurements, the results of Fig. 4 and Fig. 5 can be extended, provided there are auxiliary observations made with an independent phase center. The auxiliary observations track the power variations of the interferer and thus can be used to provide relative values of interference power between measurements at the reflectarray. These estimated (also using 1000 samples) relative values are used in the relations of Equ. (17), requiring only the estimate of a single power parameter p , as before. The example shown uses 256 elements and 5210 measurements of 1000 samples each. The interferer consists of a 40 dB ASNR pulsed signal with 50 percent cycle. The iterations converge similarly to the previous examples, achieving a null depth of 39 dB.

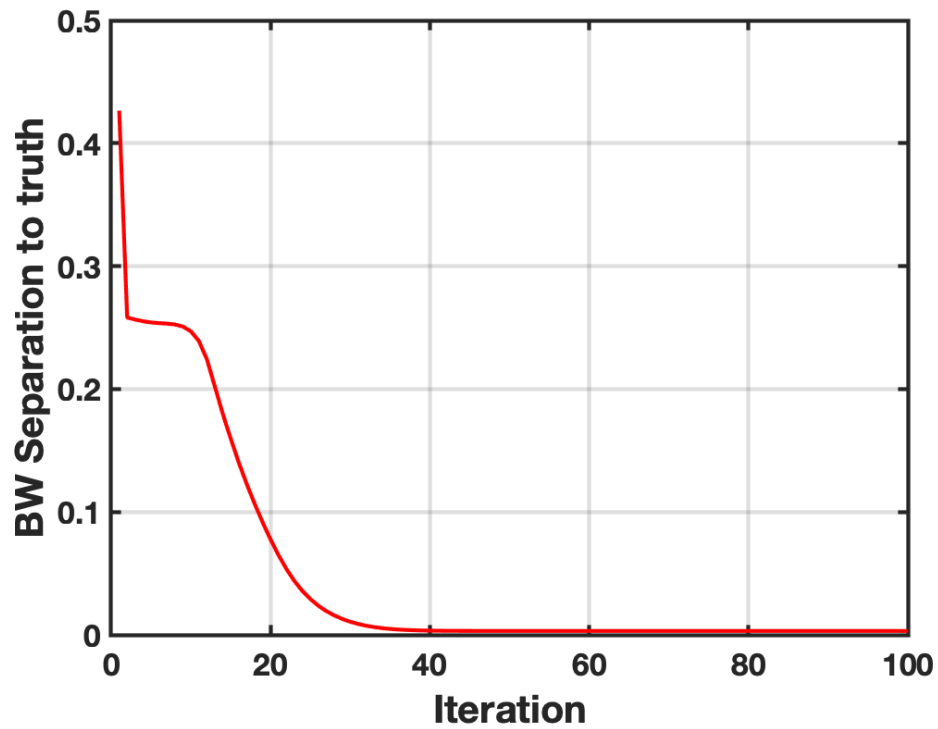


Figure 7. As a comparison with the pulsed interferer shown in Fig. 6, we show the same example without power variations in the interferer. Far fewer iterations are required for convergence, and the level of performance is better than that of Fig. 6. The achieved null depth is about 46 dB.

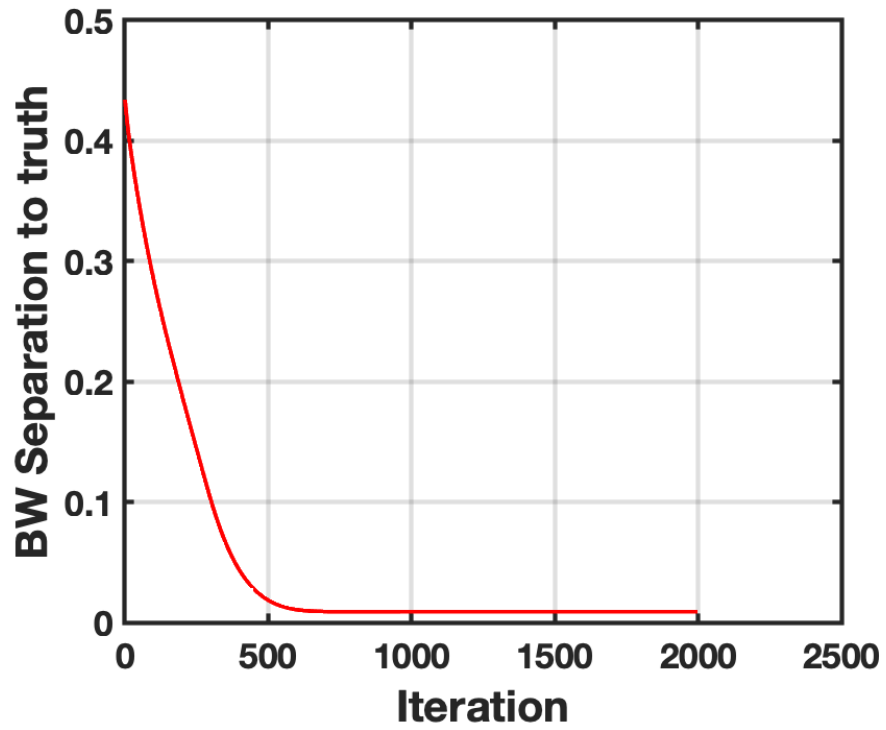


Figure 8. When the interferer pulses in a random manner, performance similar to that of Fig. 6 is achieved. In this case, the null depth is 37 dB.

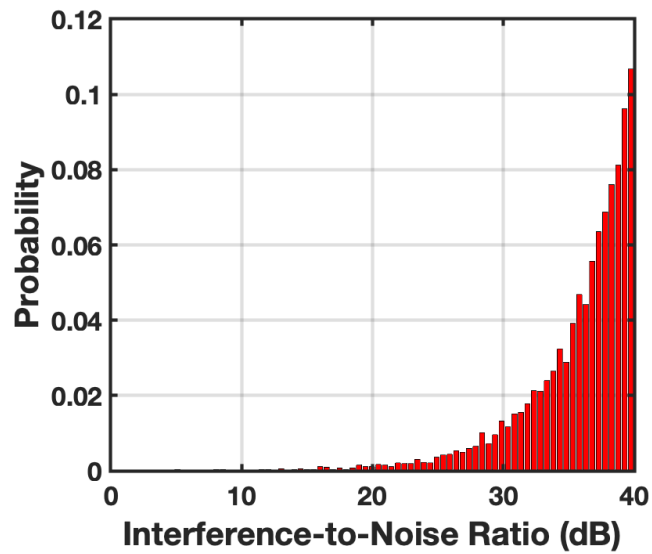


Figure 9. The histogram of interference power for the example of Fig. 8 is shown here.

5. EIGENANALYSIS USING SEQUENTIAL MEASUREMENTS

When the covariance matrix is almost rank- k , an estimation procedure similar (though more complicated) to that derived in Section 4 can be formulated. This procedure is sketched in this section. Remember, the goal is to find an iterative procedure for estimating the top k eigenvalues and eigenvectors of the almost rank- k covariance matrix using just power measurements from mostly random beams.

One can view eigenanalysis parametrically in terms of finding local (for us, around the unitary $\mathbf{U} = \mathbf{I}_n$, and hence involving Lie algebra calculations as shown below) coordinates in \mathbf{U} and \mathbf{D} for the factorization representing eigenanalysis: $\mathbf{UDU}^\dagger = \mathbf{R}$. Here, \mathbf{D} is a diagonal real matrix with only k nonunity entries, all in the first k diagonal positions. The remainder of the diagonal entries of \mathbf{D} are assumed to be fixed at unity. This factorization is highly degenerate, and hence coordinates must be chosen carefully. There is a procedure for choosing coordinates based on the concept of a homogeneous space formed from Lie groups [War83]. Conceptually, the natural coordinates are the eigenvalue entries (nonunity values) in the diagonal matrix \mathbf{D} and those coordinates on the Lie group that act nontrivially in the expression \mathbf{UDU}^\dagger . For example, the block diagonal unitaries of the form

$$\mathbf{U}_F = \begin{pmatrix} \mathbf{T} & \mathbf{0}_{k \times n-k} \\ \mathbf{0}_{n-k \times k} & \mathbf{W} \end{pmatrix}, \quad (18)$$

where \mathbf{T} is any diagonal $k \times k$ unitary and \mathbf{W} is any $n - k \times n - k$ unitary, satisfy $\mathbf{U}_F \mathbf{D} \mathbf{U}_F^\dagger = \mathbf{D}$. Thus, $(\mathbf{U} \mathbf{U}_F) \mathbf{D} (\mathbf{U} \mathbf{U}_F)^\dagger = \mathbf{UDU}^\dagger$, and hence any parameters (i.e., coordinates) in \mathbf{U}_F have no effect on eigenanalysis and are degenerate. If the nonunity entries of \mathbf{D} are distinct, these are the only degeneracies. Thus, the coordinates we seek are coordinates on unitaries subject to the equivalence relationship $\mathbf{U} \equiv \mathbf{U}'$ if and only if $\mathbf{U} = \mathbf{U}' \mathbf{U}_F$ for some \mathbf{U}_F as above. Under this equivalence relation, the resulting space is a differentiable manifold called a homogeneous space that is treated extensively in the literature in the context of Lie groups. Coordinates on the homogeneous space near $\mathbf{U} = \mathbf{I}_n$ are related to the Lie algebra of the unitary matrices.

Below, we present a sketch of the calculation of nondegenerate parameters used for gradients and Fisher matrices based on the homogeneous space model for eigenanalysis.

Assume a covariance structure of the form

$$\mathbf{R} = \mathbf{C} + \begin{pmatrix} \mathbf{I}_k & \\ & \mathbf{0}_{n-k,k} \end{pmatrix} \text{diag}(p_k) \begin{pmatrix} \mathbf{I}_k & \\ & \mathbf{0}_{n-k,k} \end{pmatrix}^\dagger = \mathbf{C} + \mathbf{V}_0 \mathbf{P} \mathbf{V}_0^\dagger, \quad (19)$$

with the implicit definitions of matrices \mathbf{V}_0 and \mathbf{P} . Below, we assume $\mathbf{C} = \mathbf{I}_n$. In this case, the form of the covariance expresses eigenanalysis of a signal subspace into the top- k eigenvectors \mathbf{e}_j , $1 \leq j \leq k$. For use below, we denote by \mathbf{e}_{lm} the matrix (of implicit dimensionality) whose only nonzero element is unity in the $(l, m)^{th}$ entry.

We can vary \mathbf{V}_0 by multiplying on the left by $n \times n$ unitaries. This moves the eigenvectors around, preserving their orthonormality. This movement is degenerate in the sense that the same movement can be accomplished by different unitaries. By carefully parameterizing unitaries near

the identity matrix, we can find nondegenerate parameters using standard arguments involving Lie algebras.

Near the identity matrix, each unitary can be written, to first order, as $\mathbf{I}_n + \mathcal{A}$, where \mathcal{A} is a skew hermitian matrix belonging to the Lie algebra of the unitaries. \mathcal{A} has block partition components given by

$$\mathcal{A} = \begin{pmatrix} \mathbf{A} & -\mathbf{B}^\dagger \\ \mathbf{B} & \mathbf{D} \end{pmatrix}, \quad (20)$$

where \mathbf{A} is in the combined span of $\{\frac{\mathbf{e}_{lm} - \mathbf{e}_{ml}}{\sqrt{2}}\}_{1 \leq l < m \leq k}$ and $\{\frac{i(\mathbf{e}_{lm} + \mathbf{e}_{ml})}{\sqrt{2}}\}_{1 \leq l < m \leq k}$; \mathbf{D} can be any element of the $(n-k) \times (n-k)$ Lie algebra of unitaries and represents most of the degenerate parameters for our problem; \mathbf{B} is in the combined span of $\{\frac{\mathbf{e}_{lm}}{\sqrt{2}}\}_{k+1 \leq l \leq n, 1 \leq m \leq k}$ and $\{\frac{i\mathbf{e}_{lm}}{\sqrt{2}}\}_{k+1 \leq l \leq n, 1 \leq m \leq k}$. \mathbf{A} does not range over the full Lie algebra of $k \times k$ unitaries. The diagonal elements are removed. These elements lead to phase scaling (unit magnitude scaling) of the new orthogonal vectors. These are degenerate parameters for our eigenanalysis application.

The number of parameters used to describe the orthonormal bases of the moved subspace is $2k(n-k)$ (for the new subspace spanned by eigenvectors; associated with \mathbf{B}) plus $k^2 - k$ for the orthonormal basis in that subspace up to scaling of the eigenvectors (associated with \mathbf{A}). Each of these parametric degrees of freedom has an associated real parameter (denoted a_{lms} or b_{lms} below) that can be adjusted to fit the observed data from sequential beams. Including the eigenvalue parameters, the total number of parameters is $2k(n-k) + k^2 - k + k = k(2n-k)$.

As a separate accounting of the number of parameters required for rank-deficient eigenanalysis, consider counting the dimensional parameters of eigenvalues and eigenvectors directly. The top eigenvector has, after normalization, $2(n-1)$ real parameters. The second requires $2(n-2)$ real parameters since an additional orthogonality constraint (orthogonal to preceding eigenvectors) is also imposed. Thus, the top k eigenvectors, after all normalizations and constraints, require $\sum_1^k (2(n-j)) = 2nk - k^2 - k$ real parameters. Along with the k real parameters for the eigenvalues, this results in a total of $2k(n-k) + k^2 = k(2n-k)$ parameters for rank-deficient eigenanalysis, as calculated above.

The modification of \mathbf{V}_0 takes the form (to first order) $\mathbf{V}_0 \rightarrow (\mathbf{I}_n + \mathcal{A})\mathbf{V}_0$. First, observe

$$\mathbf{w}^\dagger \mathcal{A} \mathbf{V}_0 = \sum a_{lm1} \frac{\bar{w}_l \mathbf{e}_m^\dagger - \bar{w}_m \mathbf{e}_l^\dagger}{\sqrt{2}} + a_{lm2} \frac{i(\bar{w}_l \mathbf{e}_m^\dagger + \bar{w}_m \mathbf{e}_l^\dagger)}{\sqrt{2}} + \sum b_{lm1} \frac{\bar{w}_l \mathbf{e}_m^\dagger}{\sqrt{2}} + b_{lm2} \frac{i\bar{w}_l \mathbf{e}_m^\dagger}{\sqrt{2}}. \quad (21)$$

Since $\mathbf{w}^\dagger \mathbf{V}_0 = (\bar{w}_1, \dots, \bar{w}_k)$, we find, to first order,

$$\begin{aligned} \mathbf{w}^\dagger \mathcal{A} \mathbf{V}_0 \mathbf{P} \mathbf{V}_0^\dagger \mathbf{w} &= \sum a_{lm1} \frac{\bar{w}_l w_m p_m - \bar{w}_m w_l p_l}{\sqrt{2}} + a_{lm2} \frac{i(\bar{w}_l w_m p_m + \bar{w}_m w_l p_l)}{\sqrt{2}} \\ &+ \sum b_{lm1} \frac{\bar{w}_l w_m p_m}{\sqrt{2}} + b_{lm2} \frac{i\bar{w}_l w_m p_m}{\sqrt{2}}. \end{aligned} \quad (22)$$

This leads to the first-order (in \mathcal{A}) expression for

$$\begin{aligned}
& \mathbf{w}^\dagger (\mathbf{I}_n + \mathcal{A}) \mathbf{V}_0 \mathbf{P} ((\mathbf{I}_n + \mathcal{A}) \mathbf{V}_0)^\dagger \mathbf{w} - \mathbf{w}^\dagger \mathbf{V}_0 \mathbf{P} \mathbf{V}_0^\dagger \mathbf{w} \\
& \approx \sqrt{2} \sum a_{lm1} \operatorname{Re}(\bar{w}_l w_m p_m - \bar{w}_m w_l p_l) - a_{lm2} \operatorname{Im}(\bar{w}_l w_m p_m + \bar{w}_m w_l p_l) \\
& \quad + \sqrt{2} \sum b_{lm1} \operatorname{Re}(\bar{w}_l w_m p_m) - b_{lm2} \operatorname{Im}(\bar{w}_l w_m p_m).
\end{aligned} \tag{23}$$

Derivatives of $\mathbf{w}^\dagger \mathbf{R} \mathbf{w}$ by p_k , a_{lms} , and b_{lms} are explicit in the first-order expansion Equ. (23).

Recall one technical issue. Namely, the top- k eigenvalues must be nonsingular (no equalities) to avoid other parameter degeneracies. In practice, this is a probability one situation.

Gauss-Newton iteration uses the gradient formed from the parameter derivatives just mentioned as well as the Fisher matrix formed from the same derivatives along with the trace-based inner products, in direct analogy to the computations shown in Equ. (17). Amplitude parameters are introduced for the square-rooted eigenvalues as in that calculation.

Conceptually, as described in Section 4, the current eigenvector estimates are rotated by unitaries to the standard form treated above, the iterative updates are applied, then the results rotated back to get the iterative updates in the original coordinates. Also, as in Section 4, an initial coarse estimated of eigenvalues and eigenvectors is provided by employing a beam scan.

Examples of the performance of rank-deficient eigenanalysis using random beams are shown in Fig. 10 and Fig. 11. The examples treat a 100-element reflectarray employing 4000 measurements of 1000 samples each. The almost rank-3 covariance has eigenvalues of 50, 45, and 40 dB. Shown in Fig. 10 is the accuracy of the eigenvector estimates, expressed in beamwidths, as a function if the iteration count. Also shown are the CRBs for each eigenvector, illustrating the ability of the Gauss-Newton estimator to achieve near optimal performance.

In Fig. 11 we see performance as measured by the CRB as a function of the number of measurements (i.e., beams) normalized by the number of elements (i.e., shifters) in the array. The knees in the curves occur roughly around a number of measurements that are 10 to 15 times the number of elements in the array. With an almost rank-3 covariance, this means the number of measurements should be at least roughly $3n_{\text{sig}} n_{\text{ele.}}$. This number is also roughly consistent with the almost rank-1 case shown in Fig. 5. There is reason to believe a crude rule of thumb like this may hold as long as the number of signals is a small fraction of the number of elements. In fact, the number of estimated parameters is $k(2n - k) \approx 2n_{\text{sig}}(n_{\text{ele.}} - n_{\text{sig.}}/2)$. One would expect performance to be poor if the number of measurements were less than this.

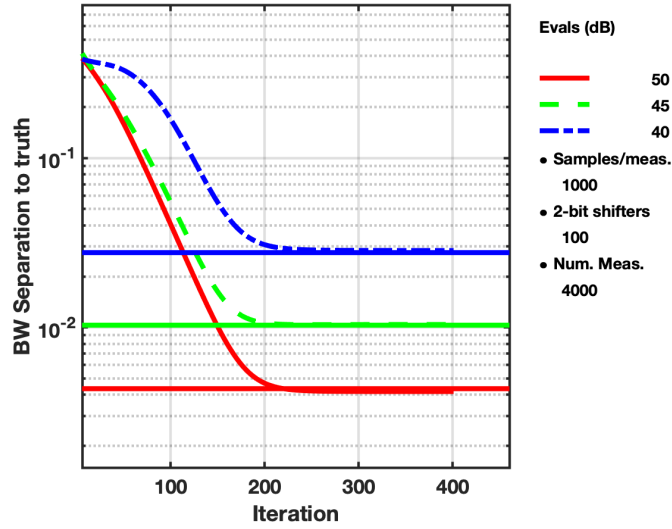


Figure 10. The sparse eigenanalysis procedure of Section 5 is exercised for a 100-element reflectarray using 4000 measurements of 1000 samples each. The true covariance has three dominant eigenvalues of 50, 45, and 40 dB. All other eigenvalues are at the unity noise floor. Also shown in the figure are CRBs for each of the eigenvalues. The Gauss-Newton iterative procedures introduced in Section 5 hit these bounds after about 200 iterations.

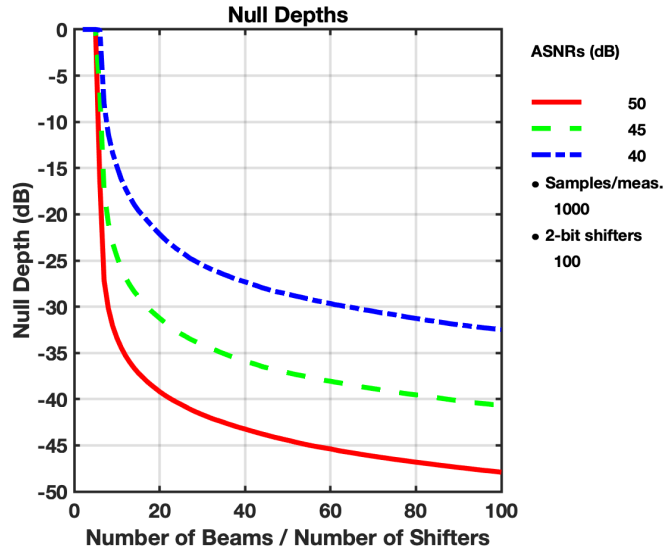


Figure 11. Since Fig. 10 indicates that the CRBs of sparse eigenanalysis are achievable, the CRBs for various numbers of measurements (number of beams) are shown as an indication of performance variations with the amount of observations. For this example, null depth increases rapidly as the number of measurements per shifter increases beyond 10. The number of measurements per shifter required for good performance tends to scale linearly with the number of significant eigenvalues as long as the eigenvalue sparsity is low as a fraction of the number of shifters.

6. DIRECT COVARIANCE ESTIMATION

In preceding sections, covariance estimation arises from parametric models of the covariance matrices. These models can be as simple as the matrix entries themselves or as more complex eigenanalysis parameters, as in the rank-deficient estimators previously treated. In this section, we consider integrating the power measurements from all weights into a matrix related to the ensemble average covariance.

Let \hat{p}_k denote the k^{th} power measurement accomplished with shifter weights \mathbf{w}_k . Over K total measurements, we form the matrix estimate $K^{-1} \sum_k \hat{p}_k \mathbf{w}_k \mathbf{w}_k^\dagger$. The ensemble average can be written as

$$\mathbf{E}_{\mathbf{w}} [(\mathbf{w}^H \mathbf{R} \mathbf{w}) \mathbf{w} \mathbf{w}^H] \quad (24)$$

where \mathbf{R} denotes the true ensemble covariance. Assume that the n -dimensional weights \mathbf{w} are drawn from a complex, circular Gaussian distribution, $\mathbf{w} \in \mathbb{C}(0, \mathbf{I}_n)$. Then, using complex Gaussian moment factoring [Ree61], the $(l, m)^{\text{th}}$ entry of Equ. (24) becomes

$$\begin{aligned} \mathbf{E}_{\mathbf{w}} \left[\sum_{jk} (w_j^H R_{jk} w_k) (w_l \bar{w}_m) \right] &= \text{tr}(\mathbf{R} \mathbf{E}[\mathbf{w} \mathbf{w}^H]) (\mathbf{E}[\mathbf{w} \mathbf{w}^H])_{lm} + \sum_{jk} \mathbf{E}[\bar{w}_j w_l] \mathbf{E}[\bar{w}_m w_k] \mathbf{R}_{jk} \\ &= (\text{tr}(\mathbf{R}) \mathbf{I}_n + \mathbf{R})_{lm}, \end{aligned} \quad (25)$$

since $\mathbf{E}[\mathbf{w} \mathbf{w}^H] = \mathbf{I}_n$. This computation suggests that

$$K^{-1} \sum_k \hat{p}_k \mathbf{w}_k \mathbf{w}_k^\dagger \quad (26)$$

could form a biased estimate of the true ensemble covariance, even if the signal environment is nonstationary. The bias does not effect the eigenvalues and eigenvectors if the noise background is the identity matrix.

Several important issues remain. One is the use of weights \mathbf{w}_k that correspond, for example, to 2-bit phase shifters, and thus are certainly not distributed as complex Gaussian random vectors. A second issue is the amount of data required to approach the ensemble covariance. Both of these issues are addressed in Fig. 12 and Fig. 13. The shifter weights are taken to be 4^{th} roots of unity, as before. As the figures show, the direct estimation procedure of Equ. (26) can successfully estimate almost rank-deficient covariances even when the interferers are nonstationary, but the number of measurements required for good estimates can be very large, especially when compared with the maximum likelihood techniques presented in Section 4 and Section 5.

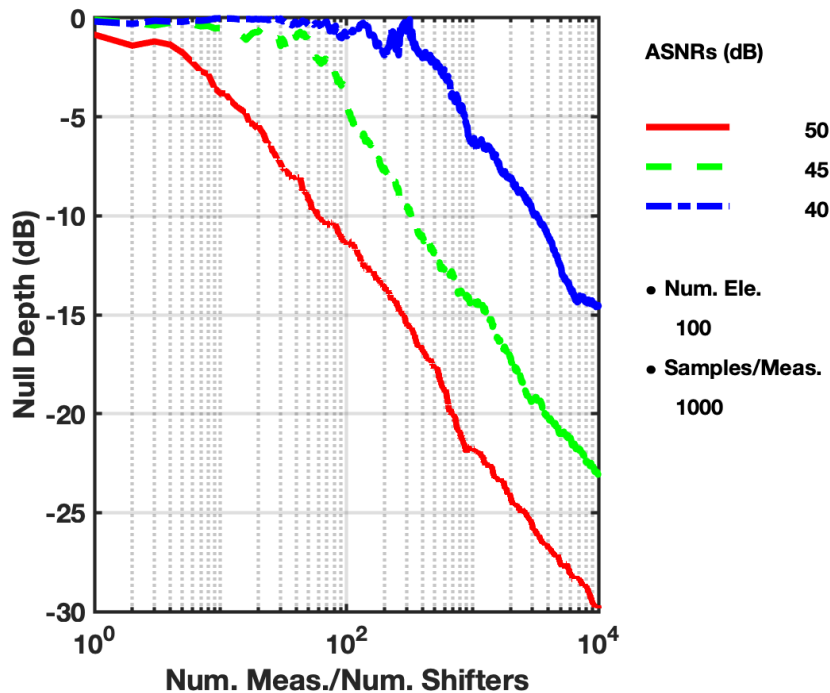


Figure 12. Direct estimates of the sample covariance as expressed by Equ. (26) are illustrated here for an example similar to those used in Fig. 10 and Fig. 11. The number of measurements per shifter is substantially greater than the number required by the sparse eigenanalysis techniques of Section 5. For example, when measurements/shifter is greater than 10, the results in Fig. 11 show good null depth, while the results here indicate poor null depth until the ratio is at least 1000.

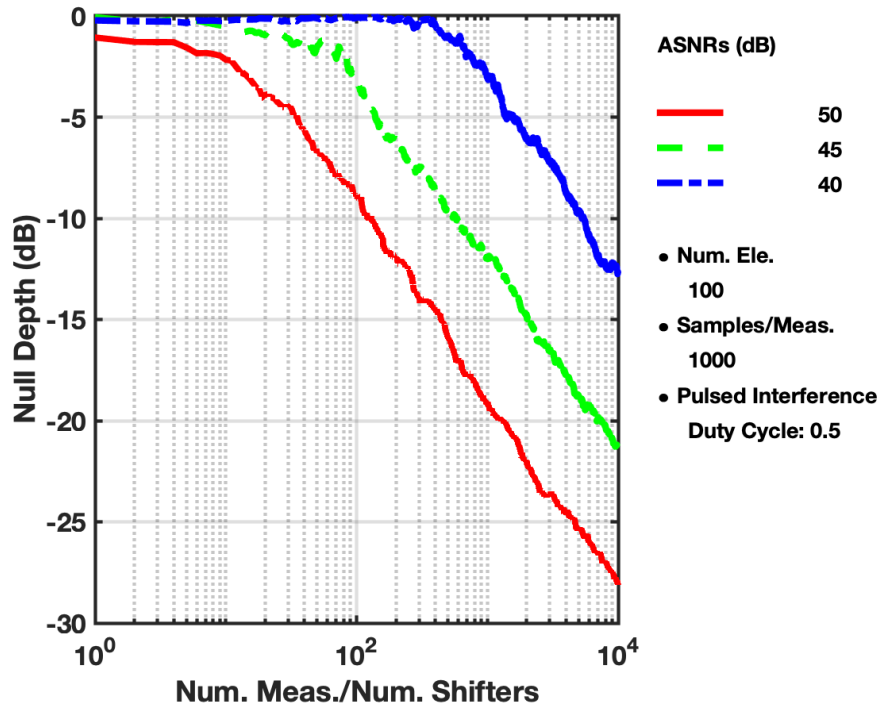


Figure 13. Although the covariance estimation procedure of Section 6 is inefficient given sparse eigenvalues, it is robust to variations in the level of interference power that occurs during measurements. The eigenvalue estimates of interferers that pulse with 50 % duty cycles is shown. There is only a few dB loss in null depth compared to Fig. 12.

This page intentionally left blank.

7. SELF-CALIBRATION FOR DISCRETE-VALUED BEAMFORMING WEIGHTS

We consider the application of beamformer weights $\tilde{\mathbf{w}}$ whose components are chosen from a finite set of unknown values. We model these weights as polynomial functions of weights \mathbf{w} with known values. The polynomial coefficients are themselves unknown and are subject to implicit estimates when multiple power measurements are made using the unknown weights. As a first goal, we establish some notation as we more precisely define the problem that is addressed.

For any specific component of the weight vectors, we let the modeled and unknown weight vectors take the discrete values $\{w_j\}$ and $\{\tilde{w}_j\}$, respectively. We explicitly treat the case when the weight components have three distinct values. In this case, polynomial expressions for the weights are derived from

$$\begin{pmatrix} a_1 & a_2 & a_3 \end{pmatrix} \begin{pmatrix} 1 & 1 & 1 \\ w_0 & w_1 & w_2 \\ w_0^2 & w_1^2 & w_2^2 \end{pmatrix} = \begin{pmatrix} \tilde{w}_0 & \tilde{w}_1 & \tilde{w}_2 \end{pmatrix}, \quad (27)$$

which is solvable when the w_j are distinct.

When the vectors $\tilde{\mathbf{w}}$ and \mathbf{w} are involved, we denote the j^{th} component of $\tilde{\mathbf{w}}$ as

$$(\tilde{\mathbf{w}})_j = \sum_{l=0}^2 a_{jl}(\mathbf{w})^l, \quad (28)$$

or, with the notation we use below,

$$\tilde{\mathbf{w}} = \sum_{l=0}^2 \text{diag}(\mathbf{a}_l) \mathbf{w}^l. \quad (29)$$

The powers, for example \mathbf{w}^k , of a vector are applied componentwise. The vector \mathbf{a}_l has j^{th} component a_{jl} . Let $D(\mathbf{a}) \stackrel{\text{def}}{=} \text{diag}(\mathbf{a})$ and let $\mathbf{R} \stackrel{\text{def}}{=} \mathbb{E}[\mathbf{z}\mathbf{z}^\dagger]$. Then the ensemble powers at the beamformer outputs are

$$\mathbb{E}[|\tilde{\mathbf{w}}^\dagger \mathbf{z}|^2] = \tilde{\mathbf{w}}^H \mathbf{R} \tilde{\mathbf{w}} = \sum_{j,k} \mathbf{w}^{j\dagger} D(\bar{\mathbf{a}}_j) \mathbf{R} D(\mathbf{a}_k) \mathbf{w}^k. \quad (30)$$

Specializing to the case of three values for each weight component, we can expand Equ. (30) as

$$\begin{aligned} \tilde{\mathbf{w}}^\dagger \mathbf{R} \tilde{\mathbf{w}} &= \mathbf{a}_0^\dagger \mathbf{R} \mathbf{a}_0 + 2 \text{Re} \left(\mathbf{a}_0^\dagger \mathbf{R} D(\mathbf{a}_1) \mathbf{w} \right) + 2 \text{Re} \left(\mathbf{a}_0^\dagger \mathbf{R} D(\mathbf{a}_2) \mathbf{w}^2 \right) \\ &+ \mathbf{w}^\dagger D((\mathbf{a}_1)^\dagger \mathbf{R} D(\mathbf{a}_1) \mathbf{w} + 2 \text{Re} \left(\mathbf{w}^\dagger D((\mathbf{a}_1)^\dagger \mathbf{R} D(\mathbf{a}_2) \mathbf{w}^2) + (\mathbf{w}^2)^\dagger D(\mathbf{a}_2)^\dagger \mathbf{R} D(\mathbf{a}_2) \mathbf{w}^2. \end{aligned} \quad (31)$$

Partial derivatives by the components of the vectors \mathbf{a}_k are given by (the notation \circ denotes the Hadamard product)

$$\begin{aligned} \partial_{\bar{\mathbf{a}}_0} \tilde{\mathbf{w}}^\dagger \mathbf{R} \tilde{\mathbf{w}} &= \mathbf{R} \mathbf{a}_0 + \mathbf{R} D(\mathbf{a}_1) \mathbf{w} + \mathbf{R} D(\mathbf{a}_2) \mathbf{w}^2 \\ \partial_{\bar{\mathbf{a}}_1} \tilde{\mathbf{w}}^\dagger \mathbf{R} \tilde{\mathbf{w}} &= \bar{\mathbf{w}} \circ \mathbf{R} D(\mathbf{a}_1) \mathbf{w} + \bar{\mathbf{w}} \circ \mathbf{R} D(\mathbf{a}_2) \mathbf{w}^2 + \bar{\mathbf{w}} \circ \mathbf{R} \mathbf{a}_0 \\ \partial_{\bar{\mathbf{a}}_2} \tilde{\mathbf{w}}^\dagger \mathbf{R} \tilde{\mathbf{w}} &= \bar{\mathbf{w}}^2 \circ \mathbf{R} D(\mathbf{a}_2) \mathbf{w}^2 + \bar{\mathbf{w}}^2 \circ \mathbf{R} D(\mathbf{a}_1) \mathbf{w} + \bar{\mathbf{w}}^2 \circ \mathbf{R} \mathbf{a}_0 \end{aligned} \quad (32)$$

The other derivatives follow in the manner $\partial_{\mathbf{a}_0} \tilde{\mathbf{w}}^\dagger \mathbf{R} \tilde{\mathbf{w}} = \overline{\partial_{\tilde{\mathbf{a}}_0} \tilde{\mathbf{w}}^\dagger \mathbf{R} \tilde{\mathbf{w}}}$ since $\tilde{\mathbf{w}}^\dagger \mathbf{R} \tilde{\mathbf{w}}$ is real-valued.

Without loss of generality in the applications, the value of \mathbf{a}_1 can be set equal to $\mathbf{1}$, the all ones vector. This holds because $\tilde{\mathbf{w}}$ can be written as $D(\mathbf{a}_1)\mathbf{q}$, where, for \mathbf{q} , \mathbf{a}_1 is set equal to $\mathbf{1}$. Then, for any power measurement, $\tilde{\mathbf{w}}^\dagger \mathbf{R} \tilde{\mathbf{w}} = \mathbf{q}^\dagger D((\mathbf{a}_1)^\dagger \mathbf{R} D((\mathbf{a}_1)\mathbf{q}$. Instead of estimating \mathbf{R} , we estimate $D((\mathbf{a}_1)^\dagger \mathbf{R} D((\mathbf{a}_1)\mathbf{q}$. This still allows us to predict accurately the measurements associated with arbitrary weights \mathbf{q} even if our weight model is inaccurate. Knowledge of \mathbf{a}_1 is not required for beamforming. Of course, in practice, \mathbf{a}_1 will be close to the all ones vector given careful choice of the nominal values of the phase shifters.

The computation of the complex Fisher matrix follows along the lines of Section 4, with the additional derivatives provided by Equ. (32). Of course, the derivatives with respect to \mathbf{a}_1 are not required. The bookkeeping of terms is straightforward as handled by a numerical computation. For convenience in computing Fisher matrices, it helps to collect some partial derivatives into $n \times l$ (number of elements by number of power measurements) arrays. This is illustrated in the case of the \mathbf{a}_0 parameters by replacing \mathbf{w} in Equ. (32) by the $n \times l$ array \mathbf{W} whose columns are the fitting weight vectors associated with each power measurement. In the term $\mathbf{R}\mathbf{a}_0$, \mathbf{a}_0 is replaced by an $n \times l$ array whose columns are all equal to \mathbf{a}_0 . The resulting $n \times l$ array, denoted $\mathbf{d}_{\tilde{\mathbf{a}}_0}$, and the analogous versions for the other array parameters are used to build entries of the complex Fisher matrix in part by computing products of the form $\mathbf{d}_{a_j} \mathbf{d}_{\tilde{\mathbf{a}}_k}^T$.

Cramer-Rao bounds based on the Fisher matrices just described are computed for the case of a single strong emitter (40 dB AINR) in white background noise, in analogy to the assessments shown in Section 4. The results are expressed in terms of the null depth achieved on the signal. This null depth is a function of the number of measurements used to estimate the covariance. Two Cramer-Rao bounds are shown. One, for the case in which the \mathbf{a}_k parameters are known precisely, and another, for which these parameters (except, remember, \mathbf{a}_1 , which is set to all ones) are unknown and must be estimated implicitly as nuisance parameters. Some results are shown in Fig. 14 and Fig. 15.

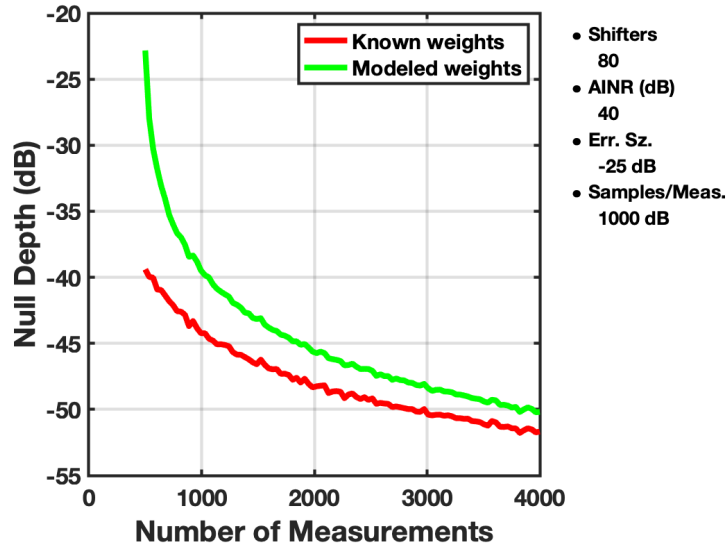


Figure 14. Shown is the null depth achieved by an array with 80 3-phase phase shifters. Both curves are based on Fisher matrices for covariance estimation. The deviations from nominal values of the phase shifters is expressed by a calibration residual of -25 dB. Null depth is shown both for the case of perfectly calibrated shifters (known weights) and for the case of unknown and uncalibrated shifters. In the latter case, the unknown calibrations are treated as unknown parameters in a Fisher matrix, with the impact of these unknown nuisance parameters a reduction of null depth. Each power measurement, using a particular set of weight/shifter values, is based on 1000 samples. The measurement weights are randomly chosen. Fluctuations in the curves are due to random changes in true shifter phases (consistent with the calibration error size) and signal array response for each curve point. It is apparent from the size of the fluctuations that these random effects are small.

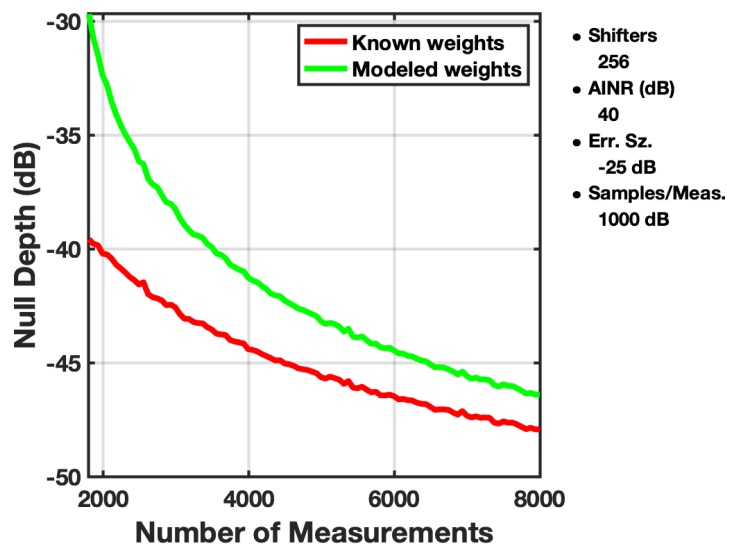


Figure 15. The format of Fig. 14 is repeated here with an increase to 256 in the number of phase shifters. The 3 to 4 increase in the number of shifters, over that in Fig. 14, requires about the same increase in the number of measurements to maintain the same level of null depth.

8. DIRECTION-FINDING USING SEQUENTIAL BEAMS

We provide a simple application of sequential power measurements to an angle-of-arrival problem associated with a planar array. The array consists of an 8×8 layout of half-wavelength-spaced phase centers that can be used to form steered beams. The beams can be steered in the directions shown in Fig. 16 and have the shapes shown in Fig. 17. Each beam can be used to form a power measurement and then these measurements can be used to estimate the angle-of-arrival of a far-field source. For the example shown here, the beams used for angle estimation are shown as green circles in Fig. 16. For illustration, the environment consists of a single source in background noise.

Write the almost rank-1 covariance \mathbf{R} over all degrees of freedom (DOF) as $\mathbf{R} = I_n + p\mathbf{v}\mathbf{v}^\dagger$, where p denotes signal ASNR provided $\|\mathbf{v}(\mathbf{u})\| = 1$. Thus, if all beamforming weights are normalized $\|\mathbf{w}\| = 1$, the noise power from the weights is also unity. The array response vector $\mathbf{v}(\mathbf{u})$ is parameterized by direction of arrival, with $v_k(\mathbf{u}) = e^{-i2\pi\mathbf{d}_k \cdot \mathbf{u}/\lambda}/\sqrt{n}$, given wavelength λ and u-vector (u_x, u_y) , $\|\mathbf{u}\|^2 \leq 1$ for a planar array in the x-y plane. The \mathbf{d}_k denote the locations of the phase centers of the planar elements. We need derivatives of the array response by the u-coordinates. Specifically,

$$\partial_{u_x} \mathbf{v}(\mathbf{u}) \equiv v_{u_x}(\mathbf{u}) = -\frac{i2\pi}{\lambda} \text{diag}((\mathbf{d})_x) \mathbf{v}(\mathbf{u}). \quad (33)$$

A Fisher matrix for parameters in the covariance \mathbf{R} has the form $F = l \text{tr}(\mathbf{R}^{-1} \dot{\mathbf{R}} \mathbf{R}^{-1} \dot{\mathbf{R}})$, where l denotes the number of samples used for power estimation in each beam. For the case of sequential beams \mathbf{w} with independent observations, the Fisher takes the form

$$F_{\alpha\beta} = l \sum_{\mathbf{w}} (\mathbf{w}^\dagger \mathbf{R} \mathbf{w})^{-2} (\mathbf{w}^\dagger \mathbf{R}_\alpha \mathbf{w}) (\mathbf{w}^\dagger \mathbf{R}_\beta \mathbf{w}) \quad (34)$$

with

$$\mathbf{R}_\alpha \stackrel{\text{def}}{=} \begin{cases} \mathbf{R}_u = p(\mathbf{v}_u \mathbf{v}_u^\dagger + \mathbf{v} \mathbf{v}_u^\dagger) & \alpha = u_x \text{ or } u_y \\ \mathbf{R}_p = \mathbf{v} \mathbf{v}^\dagger & \alpha = p. \end{cases} \quad (35)$$

The same Gauss-Newton estimation procedure used in Section 4 can be used here, based on the Fisher matrix and covariance derivatives given by Equ. (34) and Equ. (35), for the angle parameters u_x, u_y and power parameter p .

A physical definition of beamwidth is useful to interpret some of the results given below. Recall that the abstract beamwidth b between two vectors \mathbf{v} and \mathbf{w} satisfies $\cos(\pi b/2) = |\mathbf{v}^\dagger \mathbf{w}| / (\|\mathbf{v}\| \|\mathbf{w}\|)$. Thus $b = 1$ corresponds to the peak-to-null separation definition of beamwidth, at least in the abstract sense. One can translate this abstract beamwidth into a meaningful physical beamwidth by first considering the beamwidth separation of two closely spaced vectors. Write $|\mathbf{v}^\dagger(\mathbf{u}) \mathbf{v}(\mathbf{u} + \Delta \mathbf{u})| = \cos(\pi b/2)$ where b represents the separation, measured in beamwidths, between $\mathbf{v}(\mathbf{u})$ and $\mathbf{v}(\mathbf{u} + \Delta \mathbf{u})$.

Then

$$\begin{aligned}
|\mathbf{v}^\dagger(\mathbf{u})\mathbf{v}(\mathbf{u} + \Delta\mathbf{u})| &= n^{-1} \left| \sum_{k=1}^n e^{-i2\pi\mathbf{d}_k \cdot \Delta\mathbf{u}/\lambda} \right| \approx n^{-1} \left| \sum_k 1 - \frac{i2\pi\mathbf{d}_k \cdot \mathbf{u}}{\lambda} - \left(\frac{2\pi}{\lambda}\right)^2 (\mathbf{d}_k \cdot \Delta\mathbf{u})^2 / 2 \right| \\
&= 1 - \frac{1}{2} \left(\frac{2\pi}{\lambda}\right)^2 \Delta\mathbf{u} \left(n^{-1} \sum_k \mathbf{d}_k \mathbf{d}_k^T \right) \Delta\mathbf{u} \\
&\approx 1 - \frac{\pi^2 b^2}{8}, \tag{36}
\end{aligned}$$

where the last approximation uses the definition of beamwidths and the 2nd order approximation of $\cos(\pi b/2)$. In Equ. (36), the second equality follows from the assumption $\sum_k \mathbf{d}_k = 0$, which can always be arranged with a choice of origin. This choice of origin plays no role in the beamwidth metric, only the displacement of phase centers \mathbf{d}_k about their mean matters.

Identifying, at least approximately when $b \ll 1$, the last two lines of Equ. (36) gives us the beam shape near its peak as

$$b^2 \approx \frac{16}{\lambda^2} \Delta\mathbf{u}^T \left(n^{-1} \sum_k \mathbf{d}_k \mathbf{d}_k^T \right) \Delta\mathbf{u} = \frac{\Delta\mathbf{u}^T \mathbf{D} \Delta\mathbf{u}}{\lambda^2}, \tag{37}$$

where $\mathbf{D} \stackrel{\text{def}}{=} 16 \sum_k \mathbf{d}_k \mathbf{d}_k^T / n$. The beam shape at its peak-to-null spacing is given by setting $b = 1$ in Equ. (37). In explicit form, the physical beam shape satisfies

$$1 = \frac{\Delta\mathbf{u}^T \mathbf{D} \Delta\mathbf{u}}{\lambda^2}. \tag{38}$$

If $\mathbf{D} = \delta I_2$ for, say, a planar array, then the abstracted peak-to-null beamwidth has the form $\lambda/\delta^{1/2}$.

With shaped beams, the same reasoning applies and results in a beamshape given by $\mathbf{D} \stackrel{\text{def}}{=} 16 \sum_k \mu_k \mathbf{d}_k \mathbf{d}_k^T$ where the μ_k are nonnegative and satisfy $\sum_k \mu_k = 1$.

In the specific case of uniformly spaced planar, square arrays with symmetrical (under reflection about x and y axes) weightings of the phase centers, the matrices \mathbf{D} are multiples of the identity matrix.

In Fig. 18 and Fig. 19, we show the performance of the iterative Gauss-Newton estimator in terms of the normalized likelihood statistic, which can be visualized since it is two-dimensional for these direction-finding examples. The example in Fig. 18 shows a simple case with a well-behaved likelihood associated with scanned beams that have substantial overlap as in the beams shown in Fig. 16 and Fig. 17. Also shown, in Fig. 19, is the normalized likelihood for an example with scanned beams with small overlaps. In this case, we can see the lobed structure of the likelihood, which requires the initial estimate to lie on the correct lobe in order to achieve convergence to the global maximum.

In Fig. 20 we see the estimation accuracy of the Gauss-Newton procedure in the example with sparsely overlapped beams. As long as the estimator is initialized in the correct lobe of the

likelihood function, it can achieve the CRB for angle estimation as given by Equ. (34). We also see, in that figure, how suboptimal the angle estimates can be if they rely solely on the data collect in the scanned beams as opposed to data collected simultaneously at all the phase centers used to form the beams.

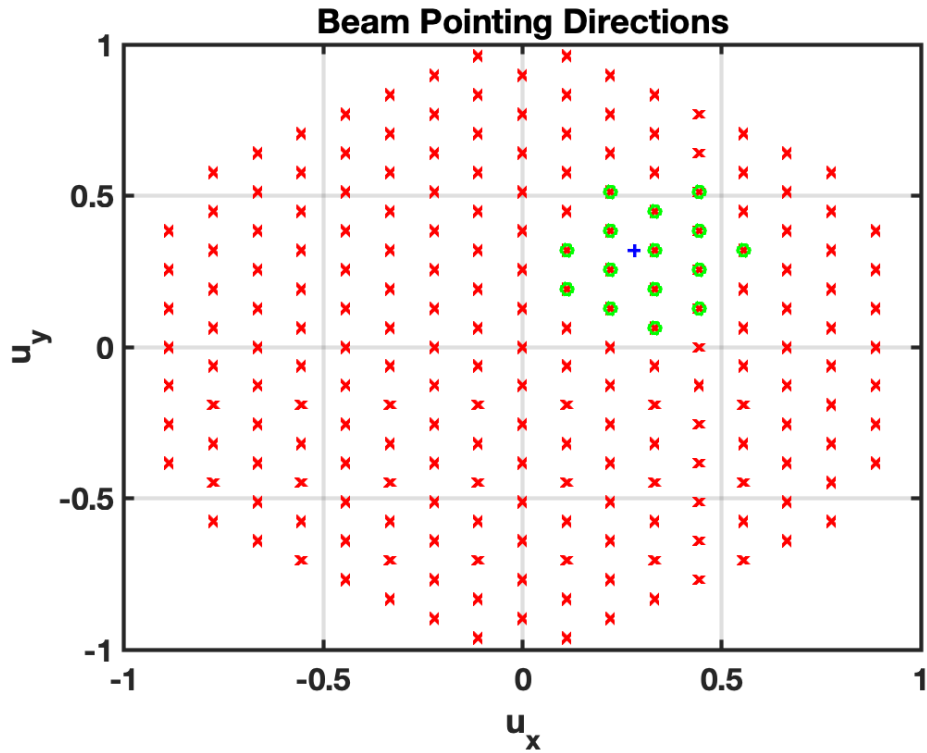


Figure 16. Shown are the scanning directions of analog beams formed using an 8×8 planar array with half-wavelength element spacing. These steered beams are used to form power estimates of the environment. The estimated powers form the basis of a maximum-likelihood direction-finding algorithm. Shown in green are the beam positions involved in estimating the direction of the source shown in blue.

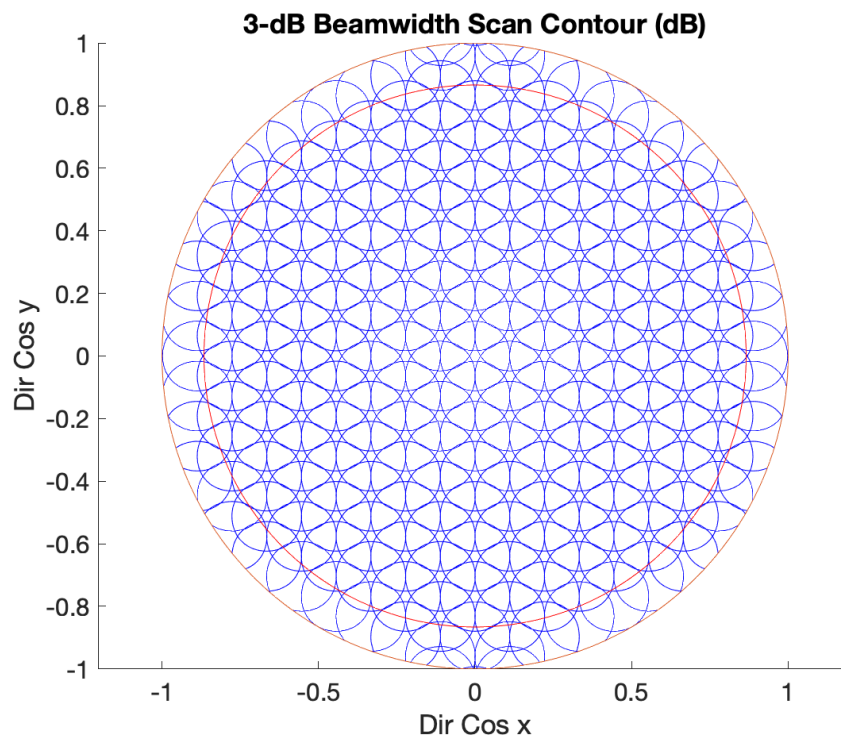


Figure 17. The beams of Fig. 16 have the shapes and overlaps shown here.

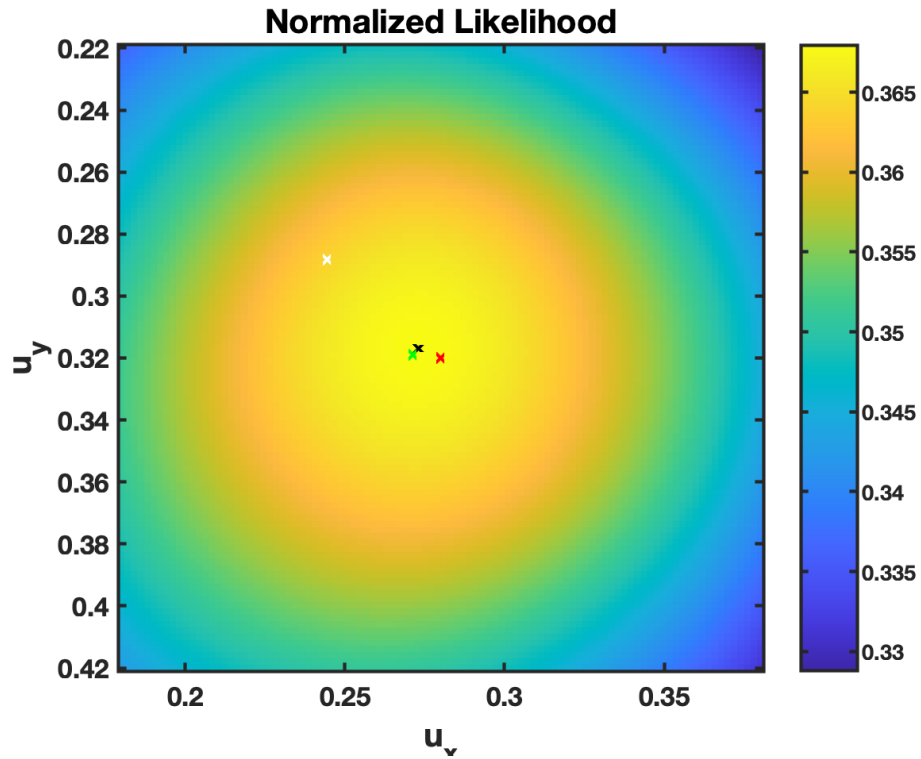


Figure 18. The maximum-likelihood procedure of Section 8 is employed using the beams and source shown in Fig. 16. Shown is the likelihood statistic. White indicates a starting estimate for the source, red indicates the true source location, black is the peak likelihood, and green shows the settling point the a Gauss-Newton iterative estimator.

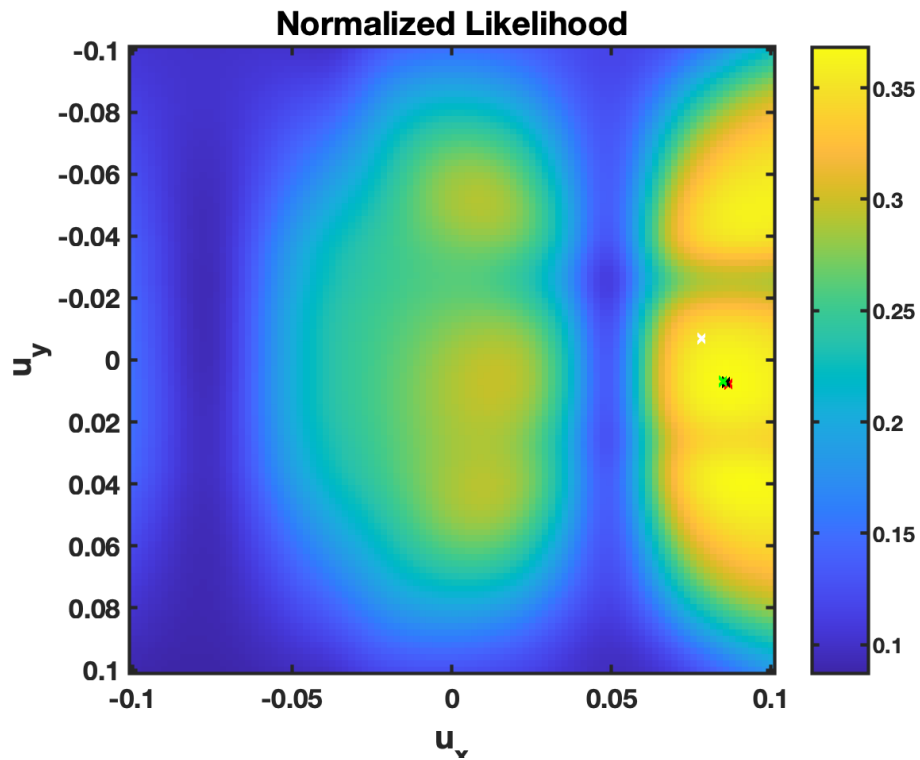


Figure 19. A more challenging example of sequential direction-finding is shown here. The likelihood function is much more complicated, based on measurements from only 6 hexagonally spaced beams (from the same 8X8 planar array) with small overlap. Note the lobe structure showing potential ambiguities in the estimates. As long as the initial estimate (white) is on the correct lobe, the Gauss-Newton estimator converges to a good solution. The colors shown have the same meaning as those in Fig. 18.

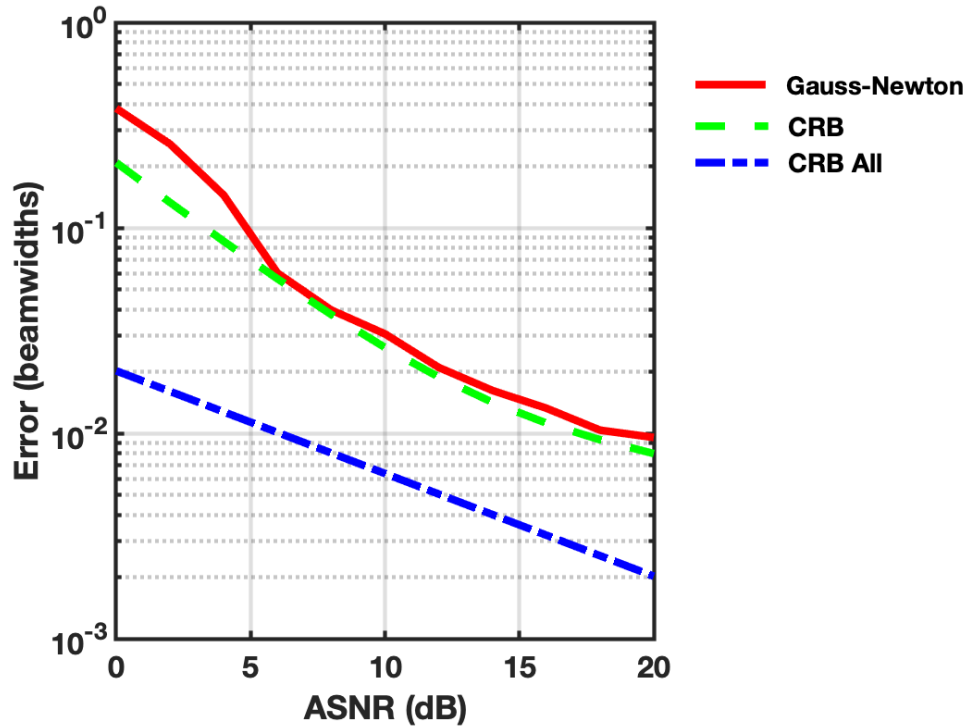


Figure 20. The performance of the iterative estimator on the example shown in Fig. 19 is shown here. The estimator hits the CRB bound. Also shown (as “CRB All”) is the CRB based on sampling the full 8×8 planar array. This shows the loss that could be suffered when using sequential scans instead of multiple, simultaneously sampled phase centers. The beamwidth error measurements are based on the physical definition of beamwidth for the particular array used in the example (8×8 as above) as derived in Section 8 from the abstract definition of beamwidth based on the normalized inner product between array responses.

This page intentionally left blank.

9. SUMMARY

We have introduced and provided an initial evaluation for a number of techniques that produce estimates of spatial covariance matrices. The estimators are constrained to measure the power at the output of a number of beam dwells. These power measurements are combined to form estimates of a spatial covariance. For reflectarrays, the main application considered in the examples shown, the spatial covariance is measured at the phase centers of the phase shifters used for beamforming. In some cases, estimates of direction-finding parameters (angles and powers) are provided instead. For this latter application, the beams used for power measurements have the physical characteristic of steered array patterns. For the cases involving just estimates of covariance, the measurement beams have mostly random patterns.

Performance is characterized in terms of the accuracy of parameter estimates and the amount of data required for a given level of accuracy. The studied parameters include eigenvalues and eigenvectors of the estimated covariance matrices and, where relevant, direction-of-arrival and signal power estimates of a source. Cramer-Rao bounds on the estimated parameters are calculated and, for some methods, are achievable in many cases. Nevertheless, even techniques that are suboptimal from the Cramer-Rao bound point of view can be interesting for reasons of complexity or robustness.

This page intentionally left blank.

REFERENCES

- [BCF⁺22] D.W. Browne, C. Chapman, K.W. Forsythe, S. Appadwedula, W. Moulder, and B. Guerriero. Phase Analog Beamforming (PhAB): FY22 RF System Line Supported Program. Technical Report LSP-374, M.I.T. Lincoln Laboratory, October, 2022.
- [MMJ⁺21] W. F. Moulder, A. C. Maccabe, S. K. Jeon, D. Stromberg, L. A. Bowen, and M. J. Silver. Deployable Electronically Scanning Reflectarray (DESRa)", FY20 RF Systems Line Supported Program. Technical Report MIT-LIN-LSP-302, M.I.T. Lincoln Laboratory, 2021.
- [Ree61] I.S. Reed. On a moment theorem for complex gaussian processes. *IRE Trans. Information Theory*, 1961.
- [War83] F.W. Warner. *Foundations of Differentiable Manifolds and Lie Groups*. Graduate Texts in Mathematics. Springer, 1983.

This page intentionally left blank.